PHYSICAL REVIEW A VOLUME 16, NUMBER 3 SEPTEMBER 1977

Fermi-hypernetted-chain methods and the ground state of fermion matter*

John G. Zabolitzky†
Argonne National Laboratory, Argonne, Illinois 60439
(Received 4 April 1977)

The convergence properties of the Fermi-hypernetted-chain method as originated by Fantoni and Rosati are investigated. Numerical results are reported for liquid ^{3}He and two model fermion liquids. It turns out that for not too high densities and not too long-ranged correlation functions the convergence to an upper bound for the ground-state energy is excellent, but that for higher densities and/or long-ranged correlation functions, it is easily possible to underestimate the upper bound if one does not apply certain convergence criteria and associated error estimates.

I. INTRODUCTION

Within the past few years the theory of infinite homogeneous Fermi systems has experienced renewed interest. This is due to the development of so-called Fermi–hypernetted-chain (FHNC) methods which allow one to estimate the expectation value of a Hamiltonian more accurately than before, as well as due to an apparent discrepancy with results obtained within the framework of perturbation methods usually called "Brueckner theory."[1] For some years it has been known[2] that variational methods tend to give more binding energy and higher saturation density than lowest-order "Brueckner" theory with standard dispersion (LOBT),[3] i.e., solutions of the Bethe-Goldstone equation with self-consistent hole and zero particle potential. In the earlier variational calculations, the expression for the expectation value of the Hamiltonian had to be truncated severely, however, such that the upper-bound property of the variational result could not be firmly established. With the newly developed FHNC techniques,[4,5] it is possible to demonstrate convergence of the expectation value within some expansion scheme[6] thus substantiating the belief that we are able to obtain an accurate upper bound for the energy. These upper bounds lie consistently below LOBT[7] essentially confirming the earlier variational results. For low and medium densities this discrepancy is of the order of magnitude which might be expected from three- and four-body terms in the perturbative approaches. It is thus of considerable interest to evaluate these three- and four-body terms. We believe that it is reasonable to hope that finally a close agreement between variational and perturbative methods will be achieved—which might then be considered a very satisfactory state of many-body theory.

In order to perform a meaningful comparison between these methods, it is necessary to demonstrate the convergence of the FHNC energy expression towards the actual expectation value corresponding to the chosen wave function. This is the main purpose of the present paper. It will be shown that for Jastrow-type[8] variational wave functions different expressions for the energy eventually converge to one another as well as to expectation values evaluated independently by means of a Fermi–Monte Carlo procedure.[9] Estimates of the error due to truncation of the FHNC expansion in terms of elementary diagrams are given. Furthermore, it is shown that if one uncritically accepts certain prescriptions for evaluating the energy in FHNC without inclusion of any elementary diagrams, the expectation value may be underestimated severely, and the saturation point may be shifted spuriously to higher densities. Therefore we strongly urge anyone performing FHNC-type calculations to perform the indicated convergence checks. Otherwise the conclusions drawn from these calculations might easily be invalid.

If we were interested specifically in nuclear matter, we would like to use the full complexity of the nuclear interaction,[10] i.e. incorporate state dependence and tensor operators.[11] Any reliable many-body theory, however, should not depend too strongly on the specific details of the force involved, but work equally well for all forces within some reasonable range. This is why we will deal with state-independent, central forces only. After the properties of different many-body methods have been established for these simplest possible forces, one might go ahead and try to incorporate more complicated features—which might, of course, be simpler in one method than in the other.

In Sec. II we will review the FHNC method and the expansion in terms of elementary diagrams. We will also introduce there the physical concepts which will turn out to be useful in the discussion of our numerical results. Different methods to estimate the convergence will be outlined. In Sec. III we will discuss the numerical procedures involved in solving the FHNC equations. Section IV

will be devoted to the application of the derived methods to three fermion liquids with state-independent central forces (namely ^{3}He), "homework" neutrons, and nuclear and neutron matter interacting via the central part of the Reid $^3s_1$ interaction, the so-called v_2 potential. In Sec. V we will summarize our findings and discuss some of their implications.

II. FHNC EXPANSION

A. Variational energy

In order to study the ground-state properties of a fermion liquid, we have to specify its Hamiltonian. We will assume throughout this paper that the particles under consideration are nonrelativistic inert particles interacting via a two-body, local, central, state-independent interaction $v(r)$; i.e., the Hamiltonian is assumed to be

$$H = T + V = \sum_i t_i + \sum_{i<j} v_{ij} = \sum_i \frac{1}{2m} p_i^2 + \sum_{i<j} v(|\vec{r}_i - \vec{r}_j|). \tag{1}$$

As a variational wave function we will assume a Jastrow-type product of a plane-wave determinant, the model state describing the noninteracting Fermi gas, and a correlation operator F consisting itself of a product of two-body correlation factors $f(r)$, i.e.,

$$|\psi(\vec{r}_1, \vec{r}_2, \ldots)\rangle = \prod_{i<j} f(|\vec{r}_i - \vec{r}_j|)\,|\phi(\vec{r}_1, \vec{r}_2, \ldots)\rangle = F|\phi\rangle. \tag{2}$$

The function $f(r)$ is assumed to be a state-independent function of only the distance between two particles, so that no operators are involved in the definition of the correlation operator

$$F = \prod_{i<j} f_{ij}. \tag{3}$$

Spin and (if present) isospin variables are understood to be included in $\vec{r}$, and integrations over $d^3\vec{r}$ will imply summation over these. The variational energy per particle of a fermion liquid,

$$E_{\text{var}} = \frac{1}{N} \frac{\langle\psi|H|\psi\rangle}{\langle\psi|\psi\rangle}, \tag{4}$$

is then completely defined by specifying the Hamiltonian (1), i.e., mass of a particle m, interaction $v(r)$, density ρ, degeneracy s (e.g., $s=2$ for ^{3}He and neutron matter, $s=4$ for nuclear matter), and correlation function (CFN) $f(r)$.

As will be shown in Sec. II D, the expectation value may rigorously be written as

$$E_{\text{var}} = T_\phi + \rho \int d^3\vec{r}\, g(r) w_2(r) + \rho^2 \int d^3\vec{r}_{12}\, d^3\vec{r}_{23}\, g_3(\vec{r}_{12}, \vec{r}_{23}) w_3(\vec{r}_{12}, \vec{r}_{23}) \tag{5}$$

with suitably defined functions w_2 and w_3, where we introduced the two- and three-body radial distribution functions,

$$\rho^2 g(r_{12}) = \rho^2 g_2(r_{12}) = \frac{N(N-1)\int d^3\vec{r}_3 \cdots |\psi|^2}{\int d^3\vec{r}_1 \cdots |\psi|^2}, \tag{6}$$

$$\rho^3 g_3(\vec{r}_{12}, \vec{r}_{23}) = \frac{N(N-1)(N-2)\int d^3\vec{r}_4 \cdots |\psi|^2}{\int d^3\vec{r}_1 \cdots |\psi|^2}, \tag{7}$$

and the Fermi kinetic energy

$$T_\phi = \tfrac{3}{5}(\hbar^2/2m)k_F^2, \tag{8}$$

with the Fermi momentum k_F given by

$$\rho = s k_F^3/6\pi^2.$$

The task of any variational calculation with a Jastrow-type wave function (2) may then be summarized as "the evaluation of the integrals (6) and (7) for a given correlation function $f(r)$." As these integrals are infinite dimensional, it is not possible to do this exactly. There are two different approaches to evaluating these expressions: In a Fermi–Monte Carlo approach[9] the infinite volume is divided into finite cells with periodic boundary conditions, and (6) and (7) are evaluated within one cell by a Monte Carlo method; in the FHNC approach (6) and (7) are expanded into an infinite series upon which partial summations are performed. By choosing different subseries to be summed, different FHNC methods are obtained. Throughout this paper we will use the FHNC formalism as derived by Fantoni and Rosati[4] (FR). We will, however, compare it with a different FHNC method developed slightly earlier by Krotscheck and Ristig[5] (KR).

If the integrals (6) and (7) could be evaluated exactly, the energy (5) would be an upper bound to the ground-state energy. As it is not possible to evaluate (6) and (7) exactly, and as it has not been demonstrated for any approximate evaluation that the approximations introduced do only raise the energy, no "variational" result, i.e., upper bound on the energy, exists to date in the strict sense. All approximation schemes necessarily introduce some error, which might be of either sign. Thus it is crucial, in order to obtain a meaningful result, to supplement the approximate upper bound (5) evaluated with approximate g_2 and g_3 with some estimate of this error. Such estimates will be given in Secs. II D and II E.

B. FHNC equations

In order to expand (6) and (7), we need some "small parameter" to expand in. As we want to deal with short-range forces $v(r)$ consisting of a repulsive core and maybe some attraction immediately outside this core, any sensible correlation function f will be small near the origin and heal to unity sooner or later such that

$$h = f^2 - 1 \tag{9}$$

is appreciable only within a restricted volume. We may thus write

$$|\psi|^2 = F^2|\phi|^2 = \prod (1+h)_{ij}|\phi|^2 = \left(1 + \sum h_{ij} + \sum h_{ij}h_{kl} + \cdots\right)|\phi|^2. \tag{10}$$

The *dynamical correlations* between particles, described by the correlation function f, therefore enter (6) and (7) only in the form of the function h, Eq. (9). There are also *statistical correlations*, however. These are described by the determinant ϕ which renders the state ψ antisymmetric. Similarly to F^2, we may expand $|\phi|^2$ in the number of exchanges between particles. Namely, we may have no exchanges, $(|\phi|^2)_0 = 1$, one exchange of two particles,

$$(|\phi|^2)_{ij} = -(1/s)l^2(k_F r_{ij}), \tag{11}$$

and so on, where we introduced

$$l(k_F r) = \frac{s}{(2\pi)^3\rho}\int_{k \le k_F} d^3k \exp(i\vec{k}\cdot\vec{r}) = 3(k_F r)^{-3}(\sin k_F r - k_F r \cos k_F r). \tag{12}$$

In this way (10) becomes a quite symmetrical expansion in the number of dynamical correlation factors, h, as well as the number of statistical correlation factors, $-l/s$. In order to evaluate (6) and (7), it is useful to introduce a graphical notation. We will adhere to the diagrammatic notation of FR, which we believe to be more adapted to the physical problem than other notations.[12] A dynamical correlation factor $h(|\vec{r}_i - \vec{r}_j|)$ is represented by a solid line joining points i and j; a statistical correlation factor $-l(k_F|\vec{r}_i - \vec{r}_j|)/s$ is represented by a dashed line joining points i and j. It will also be useful to introduce a special graphical symbol for the product $-l^2/s$ which will be represented by a helical line, Fig. 1(c). A solid dot denotes a coordinate to be integrated over, whereas an open circle denotes a fixed coordinate, such that the numerator as well as the denominator of (6) or (7) may be written as sums of such diagrams.

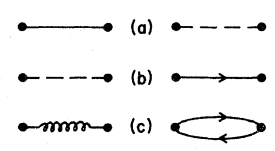

FIG. 1. Graphical elements used in the diagrammatical notation. The left-hand side shows the notation of Ref. 4 used also here. The right-hand side shows the notation of Ref. 12.

FIG. 2. Bose chain diagrams.

The main result of FR may then be summarized: the denominators of (6) and (7) cancel against the unlinked and factorizable parts of the numerators to order $1/N$. Expressions (6) and (7) are then equal to the sum of all linked, irreducible diagrams constructed according to the following rules:

(a) Each point is an extremity of at least one solid line. (b) The dashed and helical lines can be superimposed on the solid lines. (c) The dashed lines are arranged in closed polygons and there are no common points between one polygon and another; each polygon has a multiplicative factor $-2s$. (d) No helical line has a common point with another helical or dashed line.

The value of each diagram has to be divided by its symmetry number,[4,13] which will be discussed below.

This beautiful result is quite useless, however, if it is not supplemented by a practical method to sum sufficient classes of diagrams and to group the complete set into some well-defined series whose convergence may then be investigated. Also, this grouping should be performed in such a way as to result in a convergent series of approximations if truncations are performed.

This grouping has been performed by FR following the lines of van Leeuwen, Groeneveld, and de Boer and Morita,[13] who developed a similar procedure for the pair-correlation function of classical fluids. The general ordering principle is that of "connectivity" which will be made more explicit below. Let us first consider the case of particles obeying Bose-Einstein statistics, i.e., $|\phi|^2 \equiv 1$, which may be obtained from the fermion case by taking the limit $s \to \infty$ at fixed density. All diagrams are then constructed from solid lines only. The least connected diagrams contributing to (6) are those of "chain" type, Fig. 2, which are generated by a simple series connection of h bonds. We concentrate here on the expression for (6). The open

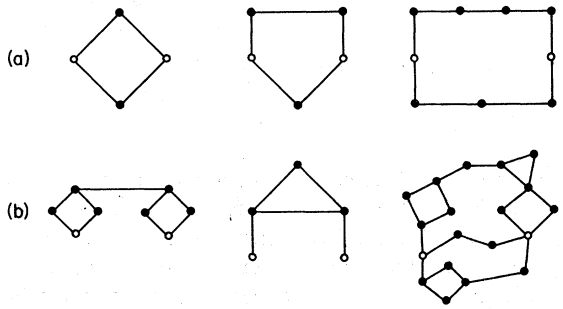

FIG. 3. Bose hypernetted-chain diagrams.

dots represent the two external points which are not integrated over, whereas the solid dots represent the field points which are integrated over. The $1+h=f^2$ factor connecting the external points is always omitted in the figures. In the next step parallel connections of chains are generated, Fig. 3(a), which then again may be connected in series-parallel, and so on, Fig. 3(b). This set of diagrams constitutes the well-known hypernetted-chain approximation[14] (HNC) for Bose systems and may be summed by means of the integral equation

$$G(r_{12})=\rho\int d^3\vec{r}_3[f^2(r_{13})e^{G(r_{13})}-1]\times[f^2(r_{23})e^{G(r_{23})}-1-G(r_{23})]. \quad (13)$$

In HNC the two-body radial distribution function (RDF) is then given by

$$g(r)=f^2(r)e^{G(r)}, \quad (14)$$

and the three-body RDF by

$$g_3(\vec{r}_{12},\vec{r}_{13})=f^2(r_{12})e^{G(r_{12})}f^2(r_{13})\times e^{G(r_{13})}f^2(r_{23})e^{G(r_{23})}. \quad (15)$$

While HNC sums a vast number of diagrams, it certainly does not sum all diagrams. It does sum, however, the longest-range, i.e., least connected, contributions to the RDF. If the h function is of range a, then for not too low density a chain of n h functions will be of range na, such that the chain-type contributions are not converging and need to be summed in a closed way. Similarly, the modification of the h bonds due to the hypernets will not be small in general, so that one has to sum these also in a closed way as done by the HNC integral equation (13).

Opposed to this behavior of the HNC-type diagrams are the four-, five-, . . . , n-point "elementary" diagrams. Consider the four-point "basic" diagram shown in Fig. 4(a). Because of the highly connected nature of this diagram, its numerical value will fall off rapidly if the distance between the two external points is increased. Similarly, the elementary diagrams generated from Fig. 4(a) by replacing each h bond by a "superbond"

$$S(r)=f^2(r)e^{G(r)}-1, \quad (16)$$

some of which are shown in Fig. 4(b), fall off rapidly. The sum $E(r)$ of the elementary diagrams will not only contribute to the RDF, but also occur within any HNC diagram. This may be conveniently taken into account by adding $E(r)$ to all $G(r)$ in the exponentials in (13)–(16).[13,15] One then has to solve (13) again, after evaluating $E(r)$ from the superbonds $S(r)$. This constitutes the HNC/4 approximation. As a modification of the HNC/4 approximation, one may perform an additional partial summation. As the $G(r)$ will be modified from the second solution of (13), the superbond $S(r)$, Eq. (16) will be changed and differ from the one used to calculate $E(r)$. In addition, $E(r)$ itself is added to $G(r)$ in (16). One may therefore require (13) to be solved self-consistently with the evaluation of $E(r)$ using (16). This self-consistency will sum a larger class of elementary diagrams. It is not clear, however, if this should be preferred to any other arrangement of the elementary diagrams, provided one uses the superbond (16) and not $h(r)$ itself as bond.

In the next order of approximation the five-point basic diagrams, Fig. 5, should be included where again a contribution to $E(r)$ is calculated from the basic pattern, Fig. 5, employing the superbonds $S(r)$ in place of each solid line. Going beyond this HNC/5 approximation one may, in principle, carry the

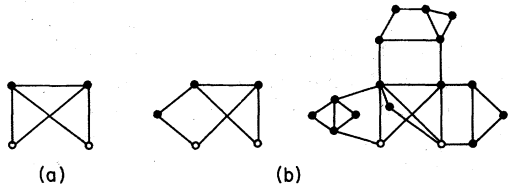

FIG. 4. Bose elementary diagrams: (a) Four-point basic diagram, (b) examples of elementary diagrams generated from (a).

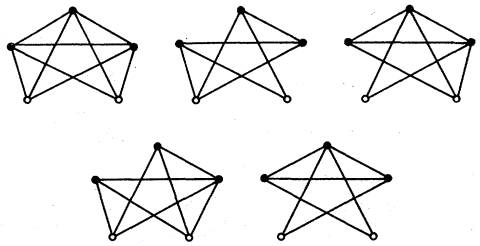

FIG. 5. Bose five-point basic diagrams.

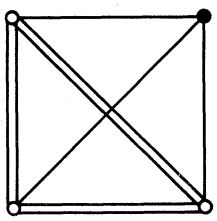

FIG. 6. Direct contribution from Fig. 4(a) to the three-body radial distribution function.

expansion in terms of basic diagrams to any desired order and investigate the convergence properties. In this way one takes into account increasingly connected contributions and finally exhausts all linked irreducible diagrams. It is on this connectedness of the higher-order terms that the hope for convergence of this series rests. For Bose systems the convergence up to HNC/5 has been demonstrated.[16]

Besides the contribution to the exponentials there is an additional contribution[16,17] of the elementary diagrams to the three-body RDF (15) shown in Fig. 6. The double bars represent the factors written down in Eq. (15), whereas the solid lines represent again the superbond S, Eq. (16). This contribution should be an integral part of any HNC/4 calculation, but has usually been omitted as was pointed out by R. Smith.[16] Also there will be similar contributions from five- and more point elementary diagrams.

The grouping of diagrams discussed in the preceding paragraphs was inspired by the physical idea of connectedness which will render higher-order terms small. There is, however, another feature inherent in this classification: the higher-order terms are increasingly difficult to compute. Whereas HNC involves only three-dimensional integrals, the four-point basic diagram, Fig. 4, implies a six-dimensional integral, the five-point diagrams, Fig. 5, imply nine-dimensional integrals, and so on. Moreover, the number of basic diagrams with n points increases rapidly with n.[16] It is therefore not feasible to include many more higher orders of basic diagrams. This is another reason why independent means to estimate the convergence in terms of basic diagrams included must be obtained: One cannot compute enough terms in this expansion to establish definitely its convergence.

Let us return now to the fermion case. As shown by FR it is possible to proceed along exactly the same lines introducing only technical complications. Essentially the task is to generalize the integral equation (13) such that the additional diagrams due to the presence of exchanges are summed also. The complication is that the rules (a)–(d) mentioned above need to be observed, which renders the topological analysis somewhat complicated. The problem was solved by FR giving the set of coupled nonlinear integral equations

$$G_{ss}(r_{12}) = \rho \int d^3\vec{r}_3 \,[\alpha(r_{13}) + G_{ss}(r_{13})]P(r_{23}), \tag{17a}$$

$$G_{sh}(r_{12}) = \rho \int d^3\vec{r}_3 \{\alpha(r_{13})\beta(r_{23}) - \gamma(r_{13})\gamma(r_{23}) + [\gamma(r_{13}) + G_{sh}(r_{13})]P(r_{23})\}, \tag{17b}$$

$$G_{hh}(r_{12}) = \rho \int d^3\vec{r}_3 \{\gamma(r_{13})\gamma(r_{23}) - \alpha(r_{13})\beta(r_{23}) + [\beta(r_{13}) + G_{hh}(r_{13})]P(r_{23})\}, \tag{17c}$$

$$G_{dd}(r_{12}) = \rho \int d^3\vec{r}_3 \,[-(1/s)l(k_F r_{13}) + \delta(r_{13}) + G_{dd}(r_{13})]\delta(r_{23}), \tag{17d}$$

$$\alpha(r) = f^2(r) \exp[E_{ss}(r) + G_{ss}(r)] - 1 - G_{ss}(r), \tag{18a}$$

$$\gamma(r) = f^2(r)[E_{sh}(r) + G_{sh}(r)] \exp[E_{ss}(r) + G_{ss}(r)] - G_{sh}(r), \tag{18b}$$

$$\beta(r) = f^2(r)\{-(1/s)l^2(k_F r) + E_{hh}(r) + G_{hh}(r) + [E_{sh}(r) + G_{sh}(r)]^2 - s[E_{dd}(r) + G_{dd}(r)]^2 + 2l(k_F r)[E_{dd}(r) + G_{dd}(r)]\}$$
$$\times \exp[E_{ss}(r) + G_{ss}(r)] - G_{hh}(r), \tag{18c}$$

$$\delta(r) = f^2(r)[E_{dd}(r) + G_{dd}(r) - (1/s)l(k_F r)] \exp[E_{ss}(r) + G_{ss}(r)] + (1/s)l(k_F r) - G_{dd}(r), \tag{18d}$$

$$P(r_{ij}) = \alpha(r_{ij}) + 2\gamma(r_{ij}) + \rho \int d^3\vec{r}_k [\alpha(r_{ik})\beta(r_{jk}) - \gamma(r_{ik})\gamma(r_{jk})]. \tag{18e}$$

If we put all $E_{xy} = 0$, this set of equations sums all diagrams of HNC type where the bonds may represent either dynamical or statistical correlation factors. The solution of (17) and (18) enables one then to evaluate the two-body RDF in the Fermi-hypernetted-chain (FHNC) approximation

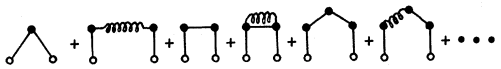

FIG. 7. Fermi-chain diagrams in G_{ss}.

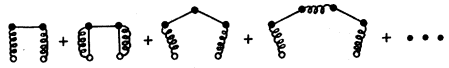

FIG. 9. Fermi-chain diagrams in G_{hh}.

$$g(r)=f^2(r)\{1-(1/s)l^2(k_Fr)+E_{hh}(r)+G_{hh}(r)+[E_{sh}(r)+G_{sh}(r)]^2+2[E_{sh}(r)+G_{sh}(r)]-s[E_{dd}(r)+G_{dd}(r)]^2$$
$$+2l(k_Fr)[E_{dd}(r)+G_{dd}(r)]\}\exp[E_{ss}(r)+G_{ss}(r)]. \tag{19}$$

Let us generate a few simple diagrams by iterating (17) and (18). The indices on the G functions (ss, sh, hh, dd) refer to the exchanges taking place at the two outer points of the corresponding diagrams. If we start iterating by setting $G_{xy}=0$, evaluate (18), and iterate (17a), diagrams with no exchanges, i.e., solid lines only on both ends, are generated, Fig. 7, which are part of the chain approximation to G_{ss}. Correspondingly, Eq. (17b) generates the chain approximation for G_{sh} having no exchange on one end and double exchange on the other end, Fig. 8. Equation (17c) generates the diagrams having double exchange on both ends, Fig. 9, while (17d) generates diagrams with single exchange on both ends, Fig. 10. One may easily write down all these diagrams by formally iterating the linear integral equations (17) and translating the result at each step into diagrammatic notation. Thus the Fermi-chain approximation is obtained by just solving once the linear systems (17). In this approximation all products of G functions including those implicit in the exponential have to be deleted from (19).

Going beyond the Fermi-chain approximation, one may solve (17) and (18) self-consistently, i.e., the full nonlinear, coupled system. This amounts in diagrammatic language to replacing each graphical element of a given exchange type by its corresponding "superbond" in the diagram forming $g(r)$. For example, all occurrences of simple helical lines will be replaced by the sum of all allowed structures having a double exchange on both ends, all solid lines will be replaced by the sum of all hypernets with solid lines only at both extremities, and so on. Equation (17) and (18) take proper care of each diagram being counted exactly once. As an example let us construct the three-body RDF. Starting from the Bose expression, Eq. (15), with $G\equiv G_{ss}$, which is diagrammatically depicted in Fig. 11(a), we put in all possible types of exchanges. In lowest order, i.e., using only simple $-l^2/s$ or $-l/s$ bonds and none of the $G_{sh,hh,dd}$ functions, we get three permutations of Fig. 11(b) and Fig. 11(c). Having obtained some approximation to the G_{xy} functions, already the "Bose" part (15) with $G=G_{ss}$ is modified, because it contains exchanges between field points by virtue of (17a) and (18). Also the $-l^2/s$, Fig. 11(b), is replaced by the sum

$$-(1/s)l^2(k_Fr)+E_{hh}(r)+G_{hh}(r)+[E_{sh}(r)+G_{sh}(r)]^2$$
$$-s[E_{ss}(r)+G_{dd}(r)]^2+2l(k_Fr)[E_{dd}(r)+G_{dd}(r)], \tag{20}$$

Fig. 12(a). The diagrammatic notation deviates here slightly from FR in that the lowest-order term is included also. The single exchange $-l/s$, in Fig. 11c, is replaced by

$$-(l/s)(k_Fr)+E_{dd}(r)+G_{dd}(r), \tag{21}$$

Fig. 12(b). Finally there is a new type of bond,

$$E_{sh}(r)+G_{sh}(r), \tag{22}$$

which generates six diagrams of type Fig. 12(c), six diagrams of type Fig. 12(d), three diagrams of type Fig. 12(e), and six diagrams of type Fig. 12(f). This list enumerates all diagrams contributing to g_3 in FHNC. All possible exchanges of the three external particles have been enumerated explicitly, and exchanges between field points are taken care of by solving (17) and (18) for the G_{xy}. We do not give the explicit formula for g_3 as this is rather lengthy, but it can trivially be constructed from (15) with $G=G_{ss}$ and (20)–(22). For all of this discussion we have $E_{xy}=0$, i.e., no elementary diagrams were taken into account. The FHNC approximation is thus defined by solving (17) and (18), evaluating the two-body RDF via (19) and the three-body RDF as discussed.

C. Elementary diagrams: The FHNC/4 approximation

Just as it was possible to go beyond the HNC approximation for Bose systems by calculating

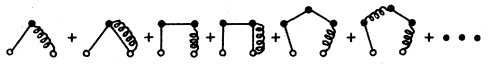

FIG. 8. Fermi-chain diagrams in G_{sh}.

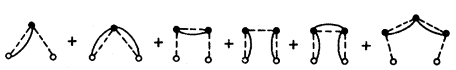

FIG. 10. Fermi-chain diagrams in G_{dd}.

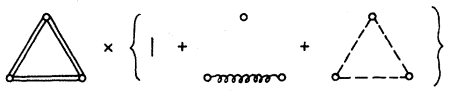

FIG. 11. Lowest-order approximation to the three-body radial distribution function.

the sum $E(r)$ of elementary diagrams from the four-point basic diagram Fig. 4(a), it should be possible to go beyond the FHNC approximation. There will be many more basic diagrams now than just Fig. 4(a) as we have to accommodate the different possible exchanges as well as the dynamical correlation factor. In fact there are 35 numerically different basic diagrams to evaluate. Employing only the simple exchanges, $-l/s$ and $-l^2/s$, we get in addition to Fig. 4(a) the seven diagrams of Fig. 13. Figures 4(a) and 13(f) contribute to E_{ss}, Figs. 13(a) and 13(e) contribute to E_{hh}, Figs. 13(b) and 13(d) contribute to E_{dd}, and Figs. 13(c) and 13(g) contribute to E_{sh}. It is not very useful, however, to calculate these diagrams in such a low-order procedure. We want to evaluate the four-point basic diagrams self-consistently with solving the FHNC equations (17) and (18) in order to take into account terms like those shown in Fig. 14. Again the argument rests on the connectedness of the contributions: Chain (or all FHNC) type contributions are not necessarily small compared to the h or l bonds; thus one should sum all these contributions. Another argument rests on the normalization of the wave function: One may easily pick long-ranged CFN's f such that in lowest order the normalization of the wave function is grossly violated,

$$\rho \int d^3\vec{r}\,[g(r)-1]\left(1-\frac{1}{s}l^2(k_F r)\right)\neq 0,$$

with $g(r)=f^2(r)$. The FHNC-type contributions will therefore strongly modify $g(r)$, and one should also take into account the corresponding modification of the bonds within the basic diagrams. This leads to the introduction of "superbonds," as was also suggested by FR,

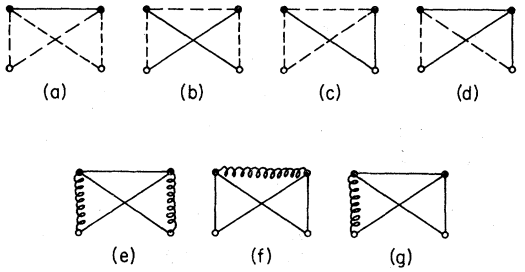

FIG. 13. Four-point basic diagrams in FHNC/4 without using S_{sh} bonds.

$$\begin{aligned}
S_{ss}(r) &= f^2\exp[E_{ss}(r)+G_{ss}(r)]-1,\\
S_{sh}(r) &= [1+S_{ss}(r)][E_{sh}(r)+G_{sh}(r)],\\
S_{hh}(r) &= [1+S_{ss}(r)]\{-(1/s)\,l^2(k_F r)+E_{hh}(r)+G_{hh}(r)\\
&\qquad +[E_{sh}(r)+G_{sh}(r)]^2-s[E_{dd}(r)+G_{dd}(r)]^2+2l(k_F r)[E_{dd}+G_{dd}]\},\\
S_{dd}(r) &= [1+S_{ss}(r)][-(1/s)\,l(k_F r)+E_{dd}(r)+G_{dd}(r)].
\end{aligned} \tag{23}$$

Each line in Figs. 4(a) and 13 will be replaced by the corresponding superbond. In addition there are 27 diagrams involving the S_{sh} bond, some of which are shown in Fig. 15. The diagram Fig. 15(d) does *not* need to be calculated separately, as its numerical value is equal to that of Fig. 15(b); whereas Fig. 15(b) contributes to E_{sh}, Fig. 15(d) contributes to E_{hh}. Similar symmetries were utilized to get down to the total number of 35 diagrams. As mentioned in the previous subsection, the values for each diagram have to be divided by the symmetry number for the diagram. The symmetry number is the number of exchanges possible between field points which do *not* generate a topologically differ-

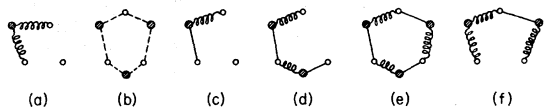

FIG. 12. Higher-order contributions to the three-body radial distribution function in FHNC.

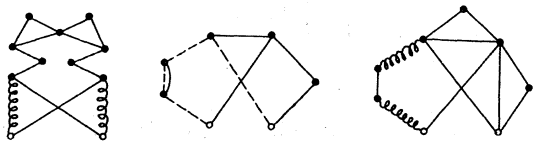

FIG. 14. Some elementary diagrams generated from Fig. 13.

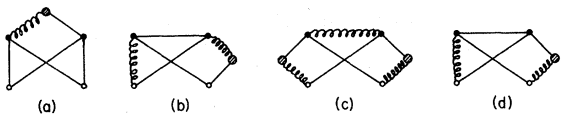

FIG. 15. Some four-point basic diagrams in FHNC/4 using S_{sh} bonds.

ent diagram. For example the symmetry numbers for the diagrams of Fig. 13(a)–13(g) are 2, 1, 2, 1, 1, 2, 1, respectively.

In this way complete hypernetted chains are inserted into the four-point basic diagrams producing a vast number of four-, five-, up to infinite-point elementary diagrams. Inserting the resulting E_{xy} functions into Eqs. (17)–(22) produces then all FHNC diagrams where one or more bonds are replaced by elementary diagrams, e.g., Figs. 14 and 16. Summing all these diagrams constitutes the FHNC/4 approximation. Also, however, the superbonds (23) will be modified such that one evaluates diagrams like Fig. 17 if one calculates the E_{xy} a second time and again solves (17) and (18). These contributions are, however, again much more connected than, e.g., Fig. 16, let alone FHNC diagrams. This is why we expect this self-consistency iteration to converge extremely fast, which will indeed turn out to be true usually. It remains questionable, however, if one should perform this additional self-consistency. There will be contributions of the same order of magnitude from basic diagrams involving five or more points. It is not clear that one should single out the special set summed by the self-consistency procedure.

Thus we obtain in complete analogy to the Bose case the FHNC/4 approximation: Solve (17) and (18) with inclusion of the four-point basic diagrams for E_{xy}, calculated from the superbonds (23). The two-body RDF is evaluated from (19) again, and all of the discussion in the preceding paragraph of the three-body RDF applies. However, we have $E_{xy} \neq 0$ now, and in (15) we have $G = G_{ss} + E_{ss}$.

Also in analogy to the Bose case, there is an additional complication, namely the direct contribution of the elementary diagrams to the three-

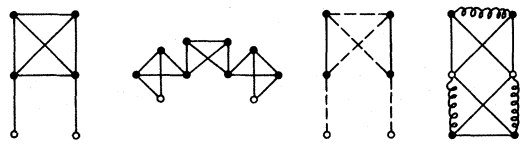

FIG. 16. Some contributions to the two-body radial distribution function if the elementary diagrams are inserted into Eqs. (17)–(19).

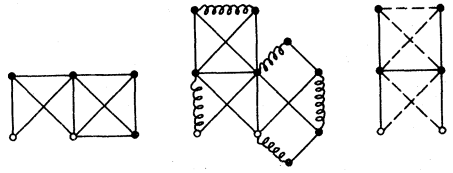

FIG. 17. Some diagrams generated by self-consistent evaluation of the elementary diagrams.

body RDF, Fig. 6. There are trivial contributions from the E_{xy} to g_3 via (15) (with $G = G_{ss} + E_{ss}$), (20)–(22). From the single Boson diagram, Fig. 6, there are generated however 99 different diagrams corresponding to different exchanges of the four particles with one another or with other field points. There is a simple way to generate all these diagrams: replace each double bar in Fig. 6 by the full $g(r)$, Eq. (19), each solid line by $g(r) - 1$, and omit all contributions which are forbidden according to the diagram rules. This procedure has been implemented in the form of a computer program and yields 161 topologically different diagrams. As in the case of Fig. 15(b) and 15(d) some of these are numerically equal such that we arrive at the final number of 99 diagrams to compute, a few of which are shown in Fig. 18. The number of diagrams for g_3 is much greater than the number for the E_{xy} because one less point is integrated over. The symmetry of the diagrams is correspondingly reduced, and a lot of formerly equal diagrams become different. Of course all these diagrams are computed from the superbonds (23) after solution of the FHNC/4 problem. This completes the definition of the FHNC/4 approximation.

Is it possible to go beyond the FHNC/4 approximation? In the Bose case there were five different five-point basic diagrams involving nine-dimensional integrals. The number of fermion diagrams contributing to E_{xy} is estimated to be several thousand, and there will be a multiple of this number contributing directly to the three-body RDF. Therefore it does not seem to be feasible to calculate these even once.

D. Expressions for the variational energy

In the preceding sections we obtained a method of calculating approximations to the two- and three-

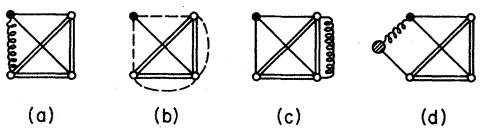

FIG. 18. Some additional contributions to the three-body radial distribution function in FHNC/4.

body RDF, Eqs. (6) and (7). In order to evaluate the variational energy (5), we need to obtain the functions w_2 and w_3.

The Hamiltonian (1) consists of a potential and a kinetic part. It is no problem to deal with the potential: there is a potential contribution to w_2,

$$w_2(r) = \tfrac{1}{2} v(r) + w_2^T(r), \quad \langle V \rangle = \tfrac{1}{2}\rho \int d^3\vec{r}\, g(r)\, v(r), \tag{24}$$

where w_2^T is a contribution from the kinetic part. w_3 is purely kinetic as we do not include three-body forces. These kinetic parts must be evaluated from the expectation value

$$-\frac{\hbar^2}{2mN}\frac{1}{\langle\psi|\psi\rangle}\sum_i \langle\phi| F\nabla_i^2 F|\phi\rangle = \langle T\rangle . \tag{25}$$

Different methods have been proposed to derive expressions for w_2^T and w_3. As one may perform partial integrations in (25), these functions are not uniquely determined.

(1) The Pandharipande-Bethe (PB) form,[15] also used by Iwamoto and Yamada,[18] is obtained by applying the differential operator in (25) to the right. This yields

$$\langle T\rangle_{\rm PB} = -\frac{\hbar^2}{2mN}\frac{1}{\langle\psi|\psi\rangle}\sum_i \langle\phi| F\left[F\nabla_i^2 + (\nabla_i^2 F) + 2(\nabla_i F)\cdot\nabla_i\right]|\phi\rangle$$
$$= T_\phi + (T_{\rm PB}^{(2)} + U_{\rm PB}) + (W_F + U_F), \tag{26}$$

where the parentheses in the second equality indicate the origin from the terms in the first equality. T_ϕ is given by (8). From $T_{\rm PB}^{(2)}$ there is a contribution to w_2^T,

$$T_{\rm PB}^{(2)} = \rho\int d^3\vec{r}\, g(r)\left(-\frac{\hbar^2}{2m}\frac{\nabla^2 f(r)}{f(r)}\right). \tag{27}$$

$U_{\rm PB}$ contributes to w_3:

$$U_{\rm PB} = \rho^2\int d^3\vec{r}_{12}\, d^3\vec{r}_{23}\, g_3(\vec{r}_{12},\vec{r}_{23}) \times\left(-\frac{\hbar^2}{2m}\frac{\nabla_2 f_{12}\cdot\nabla_2 f_{23}}{f_{12} f_{23}}\right). \tag{28}$$

W_F again gives a contribution to w_2^T:

$$W_F = \rho\int d^3\vec{r}\{f^2(r)\exp[G_{ss}(r)+E_{ss}(r)] \times[2E_{dd}(r)+2G_{dd}(r)-(1/s)l(k_F r)]\} \times\left(-\frac{\hbar^2}{m}\frac{\nabla f(r)}{f(r)}\cdot\nabla l(k_F r)\right). \tag{29}$$

Observe that in (29) the full two-body RDF does *not* occur but only that part which contains some l functions to be differentiated in accordance with (26). Similarly, the contribution from U_F to w_3,

$$U_F = \rho^2\int d^3\vec{r}_{12}\, d^3\vec{r}_{23}\,\hat{g}_3(\vec{r}_{12},\vec{r}_{23}) \times\left(-\frac{\hbar^2}{m}\frac{\nabla_2 f_{12}}{f_{12}}\cdot\nabla_2 l(k_F r_{23})\right), \tag{30}$$

is not to be used with the full three-body RDF, but those terms which do not allow for a differentiated l function are to be omitted; i.e., in Fig. 11 only diagrams (b) and (c) contribute to g_3, or in Fig. 12 only the corresponding parts from (a), (b), and (f).

(2) The Jackson-Feenberg[19] (JF) form, also used by Fantoni and Rosati,[4] is obtained by use of the Jackson-Feenberg identity,

$$\int\psi^*\nabla^2\psi\, d\tau = \frac{1}{4}\int[\psi^*(\nabla^2\psi)+(\nabla^2\psi^*)\psi - 2(\nabla\psi^*)(\nabla\psi)]\, d\tau,$$

which for fermion systems leads to

$$\langle T\rangle_{\rm JF} = -\frac{\hbar^2}{2mN}\frac{1}{\langle\psi|\psi\rangle}\sum_i\langle\phi|F^2\nabla_i^2+\tfrac{1}{2}F(\nabla_i^2 F) - \tfrac{1}{2}(\nabla_i F)^2|\phi\rangle + \frac{\hbar^2}{8mN}\frac{1}{\langle\psi|\psi\rangle}\sum_i\int F^2\nabla_i^2|\phi|^2 d\tau$$
$$= T_\phi + T_{\rm JF}^{(2)} + (W_{x2}+W_{x3}). \tag{31}$$

From $T_{\rm JF}^{(2)}$, which corresponds to the last two terms in the first line of (31), there is a contribution to w_2^T:

$$T_{\rm JF}^{(2)} = \rho\int d^3\vec{r}\, g(r)\frac{\hbar^2}{4m}\left[\left(\frac{\nabla f}{f}\right)^2 - \left(\frac{\nabla^2 f}{f}\right)\right]. \tag{32}$$

The three-body contributions from these two terms cancel exactly. From the differentiation of the square of the model state there originates a two-body term contributing to w_2^T,

$$W_{x2} = \rho\int d^3\vec{r}\,\frac{\hbar^2}{8m}\nabla^2 g(r), \tag{33}$$

where the gradient operates only on the l and l^2 functions in $g(r)$. Also there is a three-body term,

$$W_{x3} = \rho^2\int d^3\vec{r}_{12}\, d^3\vec{r}_{23}\,\tilde{g}_3(\vec{r}_{12},\vec{r}_{23}) \times\left(-\frac{\hbar^2}{4m}\frac{1}{s}\nabla_2 l(k_F r_{12})\cdot\nabla_2 l(k_F r_{23})\right), \tag{34}$$

where only those contributions of g_3 are to be used which allow for the two differentiated l functions, i.e., Fig. 11(c) or Fig. 12(b). This form of KE has been labeled FR in our earlier note.[6] The three-body term W_{x3} has been computed erroneously there, however. The correct JF energies are slightly more repulsive than the numbers reported in Ref. 6.

(3) The Clark-Westhaus[20] form, also used by Krotscheck and Takahashi,[21] is obtained by integra-

tion of the identity

$$F\phi^*\nabla_i^2(F\phi)+\text{c.c.}=F^2\phi^*\nabla_i^2\phi+\text{c.c.}+2[\nabla_i\cdot(|\phi|^2F\nabla_iF)-|\phi|^2(\nabla_iF)^2].$$

This leads to

$$\langle T\rangle_{CW}=-\frac{\hbar^2}{2mN}\frac{1}{\langle\psi|\psi\rangle}\langle\phi|F^2\nabla_i^2-(\nabla_iF)^2|\phi\rangle=T_\phi+T_{CW}^{(2)}+U_{CW}. \tag{35}$$

The two-body term is

$$T_{CW}^{(2)}=\rho\int d^3\vec{r}\,g(r)\frac{\hbar^2}{2m}\left(\frac{\nabla f}{f}\right)^2 \tag{36}$$

and the three-body term is

$$U_{CW}=\rho^2\int d^3\vec{r}_{12}d^3\vec{r}_{23}\,g_3(\vec{r}_{12},\vec{r}_{23})\frac{\hbar^2}{2m}\frac{\nabla_2f_{12}\cdot\nabla_2f_{23}}{f_{12}f_{23}}. \tag{37}$$

Several comments apply to these three different forms of the kinetic energy (KE).[22] All three forms must yield identical results,

$$\langle T\rangle_{PB}=\langle T\rangle_{JF}=\langle T\rangle_{CW}=\langle T\rangle, \tag{38}$$

if the exact RDF's are used as only rigorous algebraic manipulations and partial integration have been employed to derive them from (25). In any approximation for the RDF's, however, the equalities (38) will generally be spoiled as the manipulations done to derive (26), (31), and (35) imply different treatments of the omitted terms in g_2 and g_3. Some relations are valid trivially in any approximation scheme:

$$U_{CW}=-U_{PB}, \tag{39}$$

$$T_{JF}^{(2)}=\tfrac{1}{2}(T_{PB}^{(2)}+T_{CW}^{(2)}). \tag{40}$$

Also we have in lowest order, $G_{xy}=E_{xy}=0$,

$$T_{CW}^{(2)}=T_{PB}^{(2)}+W_F=T_{JF}^{(2)}+W_{x2}. \tag{41}$$

This last relation may be used as a check on the numerical accuracy in the integration, and also in determination of the derivatives of the CFN if these are not given analytically, but calculated numerically (see Sec. II F).

The three KE expressions each have their merits and disadvantages. In the PB prescription there will be some cancellation involved in w_2, Eq. (24), between the repulsive short-range part of the potential and the attractive second derivative, (27). The cancellation can be especially enhanced if one chooses the CFN f in a special way, see Sec. II F. Thus in the PB prescription the *sum* $\langle T\rangle+\langle V\rangle$, in its two-body part, is insensitive to the behavior of $g(r)$ for small r.[15] There is, however, a large three-body term U_{PB}.

The JF prescription yields an extremely small three-body term W_{x3} and thus is very insensitive to any approximation made for the three-body RDF. However, the cancellation between the second derivative and the potential is not complete, and thus this prescription is more sensitive to the short-range behavior of $g(r)$. In the CW prescription there is no cancellation involved for small r; thus with this expression for the KE, the total energy is very sensitive to the short-range behavior of $g(r)$. Also there is a large three-body term U_{CW}. On the other hand, this form is the simplest in structure and application and does not require the evaluation of second derivatives. Moreover, it is the only form for which one only needs to know the complete two- and three-body RDF's and does not need to know their decompositions into the various exchange parts, Eq. (19) and Figs. 11 and 12.

Differing results for the three KE values obtained with these three prescriptions are due to different treatments implied for the omitted higher-order terms in the RDF's.[17] Thus we expect *a priori* that for a given approximation to g_2 and g_3 the three numbers should agree quite well for low densities, as higher-order terms should be small there because they are multiplied by higher powers of the density, and gradually diverge from each other with increasing density. Employing better approximations for g_2 and g_3 then should move the curves towards one another again and should not matter at low densities. In other words, we conjecture that the difference between the different results for the KE is some measure for the accuracy of the whole procedure. It is a necessary (though not sufficient) condition for any approximate g_2 and g_3 to be "good" that the three approximate values for the variational energy E_{var},

$$E_{PB}=\langle V\rangle+\langle T\rangle_{PB},$$

$$E_{JF}=\langle V\rangle+\langle T\rangle_{JF},$$

$$E_{CW}=\langle V\rangle+\langle T\rangle_{CW},$$

are not too far from one another.

E. Model energies

In the previous subsections we reviewed a method to calculate approximate upper bounds to the ground-state energy per particle of fermion liquids. Though it has not been shown that the so-obtained energies are indeed upper bounds, they will lie within some error band near to the variational energy E_{var}, Eq. (4). What one also might be interested in is the exact or true ground-state energy per particle E_0 obtained from solution of Schrödinger's equation

$$H|\psi_0\rangle=NE_0|\psi_0\rangle, \tag{42}$$

where $|\psi_0\rangle$ is the true ground-state wave function. With (42) we have for *any* state $|X\rangle$ nonorthogonal to $|\psi_0\rangle$

$$\langle X|H|\psi_0\rangle = NE_0\langle X|\psi_0\rangle ,$$
$$E_0 = \frac{1}{N}\frac{\langle X|H|\psi_0\rangle}{\langle X|\psi_0\rangle} . \tag{43}$$

Within the framework of perturbation or "Brueckner" methods, one makes use of this property with $|X\rangle = |\phi\rangle$, where $|\phi\rangle$ is the model state, and obtains

$$E_0 = (1/N)\langle\phi|H|\psi_0\rangle \tag{44}$$

with the normalization $\langle\phi|\psi_0\rangle = 1$. Effectively, (44) is used there to evaluate the energy for approximate $|\psi\rangle$ substituted for $|\psi_0\rangle$. By analogy we define[23] the "model energy"

$$E_{\rm mod} = \frac{1}{N}\frac{\langle\phi|H|\psi\rangle}{\langle\phi|\psi\rangle} \tag{45}$$

to be evaluated for the Jastrow wave function (2). This energy is, of course, not supposed to be an upper bound. In fact, it may be above or below both the variational as well as the exact energy. In general, there is no definite relationship between the model energy and any other quantity as the Jastrow wave function (2) certainly does not fulfill Schrödinger's equation. If, however, the upper bound obtained from any wave function $|\psi\rangle$ is supposed to be not very much above the true ground-state energy E_0, necessarily this wave function $|\psi\rangle$ is in some sense "close" to the true ground-state wave function $|\psi_0\rangle$. Then we may view $|\psi\rangle$ as an approximation to $|\psi_0\rangle$ and evaluate the energy from (45). The "closer" $|\psi\rangle$ is to $|\psi_0\rangle$, the better should $E_{\rm mod}$ and $E_{\rm var}$ agree, and the closer should $E_{\rm var}$ be to E_0. In particular, for the most stringent upper bound obtained with the true ground-state wave function $|\psi_0\rangle$ itself, we have $E_{\rm mod} = E_{\rm var} = E_0$. If the model and variational energies differ substantially, we may thus conclude that the wave function is quite far from the exact eigenstate. The opposite does not hold true, however, as $E_{\rm mod}$ and $E_{\rm var}$ might agree accidentally.

The evaluation of (45) is quite simple once we know how to evaluate (4).[6] The only difference is that the correlation factor F, Eq. (3), is missing on the left-hand side of the matrix elements. Thus in order to obtain the RDF's corresponding to (45), we just replace everywhere F^2 by F, or f^2 by f, e.g., in Eqs. (9) and (10), etc., up to (18), (19), and (23). The only place we have to be careful is in the KE expression, as we should not apply any differential operator to the F missing on the left-hand side. It is seen immediately that the PB expression for the KE, Eq. (26), fulfills this condition. Having obtained the solution of the FHNC (or FHNC/4) equations with the $f^2 \to f$ replacement, we may evaluate the model energy from Eqs. (24) to (30), i.e.,

$$E_{\rm mod} = V_{\rm mod} + T_{\rm mod} , \tag{46}$$

$$V_{\rm mod} = \tfrac{1}{2}\rho\int d^3\vec{r}\, g_{\rm mod}(r)v(r) , \tag{47}$$

$$T_{\rm mod} = \frac{1}{N}\frac{\langle\phi|TF|\phi\rangle}{\langle\phi|F|\phi\rangle}$$
$$= T_\phi + [T_{\rm PB}^{(2)} + U_{\rm PB} + W_F + U_F]_{\rm mod} , \tag{48}$$

where in (48) the KE operator is applied to the right.

Obviously there is a different way to evaluate (48) than by applying T to the right. One may apply it to the left yielding

$$\frac{1}{N}\frac{\langle T\phi|F|\phi\rangle}{\langle\phi|F|\phi\rangle} = T_\phi\frac{\langle\phi|F|\phi\rangle}{\langle\phi|F|\phi\rangle} = T_\phi , \tag{49}$$

with T_ϕ given in (8) as $|\phi\rangle$ is an eigenfunction of T. Now Eq. (49) is exact, whereas (48) is evaluated via the FHNC or FHNC/4 approximation. The difference between these two results then is the truncation error of the approximation used, i.e., the sum of the higher-order terms omitted. For the model kinetic energy we are therefore in the singularly lucky position of knowing exactly the error due to our approximations, and moreover we know it for any given CFN f. We are thus enabled to study the convergence properties of the expansion in basic diagrams in relation to the properties of f in an unambiguous way.

F. Correlation functions

Up to now we assumed some correlation function (CFN) f to be given. As we are mainly interested in the convergence of the FHNC expansion and comparison with other results, we are not particularly concerned with minimizing the energy. On the other hand, the convergence of the basic-diagram expansion will depend on properties of the CFN, so that we need to have some reasonable range or family of CFN's. These requirements are met by the prescription developed by Pandharipande.[24] A one-parameter family of functions is constructed as solutions of the eigenvalue problem for a second-order differential equation,

$$-(\hbar^2/m)\nabla_r^2 f(r) + v(r)f(r) = \lambda f(r) , \tag{50}$$

with the lowest eigenvalue λ and the boundary conditions

$$rf(r)\xrightarrow{r\to 0} 0 , \quad f(d) = 1 , \quad f'(d) = 0 , \tag{51}$$

where d is some prescribed "range" of the CFN, $f \equiv 1$ outside d. Thus we may conveniently produce

a reasonable CFN for a given range via (50) without the necessity of doing many-parameter minimizations. Equation (50) is obtained by minimizing the lowest-order two-body energy analytically, i.e., from the Bose ($\varphi = 1$) analog of

$$\delta\rho \int d^3r\, f(r)\left(-\frac{\hbar^2}{2m}\left[\nabla_r^2 f(r)\right] + \tfrac{1}{2} v(r) f(r)\right)|\varphi(r)|^2 = 0\,,$$

$$|\varphi(r)|^2 = g_F(r) = 1 - (1/s) l^2(k_F r)\,, \tag{52}$$

where g_F is the free Fermi-gas RDF. In cases where the corrections to the lowest order are small, it is reasonable to hope that this f will provide a very satisfactory upper bound. If the corrections become large, one may still hope that (50) is not completely unreasonable, but it would be extremely surprising if one could not lower the energy by taking a different choice for f.[22] In the low-density limit this choice of CFN reproduces the exact energy[17] though it does not lead to the correct asymptotic behavior[14] of the CFN for $r \to \infty$, $f(r) \cong 1 - c/r^2$. The parameter d may be utilized in different ways. It is possible to restrict d to small values in order to obtain good convergence in the basic diagram expansion. Alternatively, one may view d as a parameter of the CFN and minimize the energy with respect to d. However, this minimization might produce misleading results if d is moved into a region of bad convergence, since in any given approximation the quality of that approximation will depend on d.

That the range of f may significantly influence the convergence properties is easily seen. As we are expanding in powers of h, Eqs. (9) and (10), some measure for the convergence will be the deviation of f from unity[2,22,25]:

$$\kappa = \rho \int d^3\vec{r}\,|[1 - f(r)]\,\varphi(r)|^2\,,$$

$$= \rho \int d^3\vec{r}\,[1 - f(r)]^2 g_F(r)\,. \tag{53}$$

It does not seem to be useful to use $h(r)$ itself in the integrand, as h may change sign, $f(r) > 1$, for some r and thus may deviate significantly from unity without the integral becoming large. Also (53) bears some analogy to the wound parameter in "Brueckner" theory if we identify $f\varphi$ with the two-body correlated wave function there. With increasing range of the CFN, κ will increase such that we expect the expansion to converge more slowly.

It has also been proposed that a state-dependent CFN f be used in (50), i.e., that allowance be made for some dependence on angular or linear momentum.[15] It has been shown,[6] however, that for such CFN's it is not possible to evaluate higher-order terms via the FHNC equations as given by (17) and (18) as these do not allow for such complicated CFN's. If one wants to introduce more complicated CFN's than (50), one first has to derive the corresponding generalization of the FHNC equations.[11]

An alternative method frequently used in the literature is to pick some analytical form for f involving a few parameters and to minimize the energy for these. The advantage of this method is that one includes higher-order terms in the minimization.[22] The disadvantages are, however, that one has to perform a cumbersome numerical minimization for the parameters, and more important, has to select one of the KE forms (26), (31), or (35). Generally, minima of the three energies evaluated with these three different prescriptions will occur for different f. Exceptions are lowest-order, i.e., (52), and an exact evaluation of the expectation value (4). Because of these problems we use only analytic CFN's given by other authors in order to compare with their results.

There is an additional advantage of (50) if we utilize the PB prescription for the KE.[15] As mentioned in Sec. II D, with this form of KE there is a cancellation involved in (24) between the potential $v(r)$ and the $w_2^T(r)$ from $T_{\rm PB}^{(2)}$, Eq. (27), for small r. If we use (50), it is seen that the sum of these two terms is constant for r less than d; i.e., the cancellation is exploited to its maximum: there is no trace whatsoever of any repulsive core within $v(r)$, so that the behavior of $g(r)$ for small r is quite irrelevant. It might seem that this is a strong argument in favor of (50) together with the PB choice of KE. However, the other terms in $T_{\rm PB}$ were neglected in this argument, and especially the fact that $U_{\rm PB}$ might become quite large and thus render the three-body RDF quite important invalidates it. Uncertainties in the JF prescription for KE due to errors in $g(r)$ for small r show up in the PB prescription due to errors in g_3 for $r < d$. This important point will be discussed below more amply in connection with our numerical results.

III. NUMERICAL PROCEDURES

A. Solution of Pandharipande's differential equation

The first step in a numerical calculation of the energy is the determination of the correlation function. If this is not given analytically, we want to solve (50). This is most conveniently done by employing a finite difference approach.[26] The unknown function f is made discrete on a linear mesh for $0 \leq r \leq d$. Making the usual substitution $u = rf$, Eq. (50) may be written as an eigenvalue problem for a symmetric, tridiagonal matrix with eigenvalue λ and eigenvector $u(r_i)$ where the r_i are the chosen mesh points. $f(r_i)$ is then given by $u(r_i)/r_i$, and

the second derivative may be evaluated using (50) again

$$-\frac{\hbar^2}{m}\nabla_r^2 f(r)\Big|_{r=r_i} = [\lambda - v(r_i)]f(r_i). \tag{54}$$

However, in order to evaluate the KE we need also the first derivative which is given by the central difference

$$f'(r_i) = [f(r_{i+1}) - f(r_{i-1})]/(r_{i+1} - r_{i-1}). \tag{55}$$

The values of the various functions for other r than the r_i may then be obtained by interpolation. As the amount of calculation involved here is only linear in the number of mesh points, it is no problem to obtain excellent accuracies. Generally, step sizes less than 0.01 fm for nuclear or neutron matter, and 0.01 Å for ^{3}He, were used. Moreover, the numerical accuracy may be checked by means of Eq. (41).

B. Radial integrals

In various places we have to perform radial integrations, e.g., to evaluate the energy, Eqs. (24), (27), etc. These radial integrals extend from zero to infinity. Though it is possible, in principle, to use some integration formula for this interval, it is not very reasonable to do so because of the oscillating l functions, Eq. (12), where one would like to have at least a few mesh points per half wave. Since the CFN's usually tend to unity quite fast with r, it is reasonable, however, to introduce some cutoff $R_{\max}$ for the radial integrals occurring in the FHNC equations (17) and (18). The only place where contributions from $r > R_{\max}$ need to be taken into account is the integral for the potential energy (24), in the case of potentials which decrease quite slowly. Here the RDF $g(r)$ is replaced by unity for $r > R_{\max}$, and the integral may be done analytically. Of course, $R_{\max}$ has to be chosen large enough that the other contributions from $r > R_{\max}$ may safely be neglected, i.e., such that the results are independent of $R_{\max}$. This usually occurs for $R_{\max}$ in the range of $10r_0$ to $20r_0$, where r_0, the mean interparticle distance, is given by

$$\tfrac{4}{3}\pi r_0^3 \rho = 1. \tag{56}$$

The remaining integrals from 0 to $R_{\max}$ must still be evaluated with some care as the integrands generally are not arbitrarily often differentiable. Let us consider the more general case of a hard-core potential with core radius r_c and a PB-type CFN, Eq. (50). Then the CFN f will not be arbitrarily often differentiable at the points r_c and d. At r_c the first derivative will not be continuous, and at d the second derivative will not be continuous. It is therefore necessary to divide the interval from 0 to $R_{\max}$ into three subintervals, from 0 to r_c, from r_c to d, and from d to $R_{\max}$. Within each of these intervals, one may then use high-order integration formulas such as Gaussian integration, where the error is proportional to some higher-order derivative of the integrand. Even if the integrand is everywhere arbitrarily often differentiable, it is advantageous to use the three subintervals as the integrand behaves quite differently in the three regions. Within some "core" (e.g., for ^{3}He) it will generally be quite flat. The intermediate range, where the variations of the potential and the CFN are most pronounced, will be most difficult to integrate, and at larger distances the integrand will again be quite flat except for the oscillations of the l functions. Even for analytically given CFN we will thus define some d, in the region $2r_0$ to $3r_0$, in order to subdivide the integration interval. Generally 10 to 15 Gaussian mesh points suffice for the interval from d to $R_{\max}$, and 15 to 20 points for 0 to d. The accuracy may again be checked by use of (41).

C. Solution of integral equations

The principal numerical problem in the present work is the solution of the system of coupled, nonlinear integral equations (17) and (18), the FHNC equations. What prevents us here from a straightforward discretization and transformation to a nonlinear system of algebraic equations is the angular integration involved in expressions of the type

$$G(r_{12}) = \rho \int d^3\vec{r}_3\, a(r_{13})b(r_{23}). \tag{57}$$

In the numerical calculation all functions involved will be known only at certain mesh points r_i corresponding to the set of Gaussian meshes introduced in the last subsection, and we desire to know G also on these same mesh points. The angular integration would involve the functions at different mesh points. Moreover, it would be extremely difficult to keep track of the special points $r = r_c$ and $r = d$ during the angular integration. All these problems are overcome by use of the convolution theorem transforming (57) into

$$G(r_{12}) = 8\rho \int k^2\, dk\, j_0(r_{12}k)\left(\int r_a^2\, dr_a\, j_0(r_a k)a(r_a)\right) \times\left(\int r_b^2\, dr_b\, j_0(r_b k)b(r_b)\right). \tag{58}$$

On the mesh $\{r_i\}$ (57) may then be written as

$$G(r_i) = \sum_{jk} c_{jk}^i\, a(r_j)b(r_k), \tag{59}$$

where the coefficients c_{jk}^i are given by

$$c^i_{jk} = 8\rho \frac{r_j r_k}{r_i} w_j w_k \int_0^\infty \frac{dk}{k} \sin(r_i k) \sin(r_j k) \sin(r_k k). \tag{60}$$

The w_i are the weight factors corresponding to the mesh points r_i obtained from the Gaussian integration formulas.

The integral in (60) may be evaluated in closed form. Again one has to be careful, however, as for very large values of k the radial integrals in (58) cannot be performed on the given mesh $\{r_i\}$. Thus we are led to introduce some cutoff (exponential, step, etc.) for the integral (60). Again the results should not depend on that cutoff within reasonable limits which indeed turns out to be true. Even without cutoff all results but the values of G_{xy} for very small r are reasonable due to some extrapolation of the integrals in (58) implicit in (60). Fortunately f^2 is extremely small for very small r such that these inaccuracies do not matter too much. All actual calculations reported here however used a cutoff in the region of $20r_0^{-1}$.

We now eliminate (18) by inserting it into (17). Discretizing on the set of Gaussian meshs and using (59), we obtain a set of coupled nonlinear algebraic equations which may be written

$$X_i(G_j) = 0, \quad 1 \leq i,j \leq M; \tag{61}$$

i.e., there are M equations and M unknowns $G_j \in \{G_{ss}(r_k), G_{sh}(r_k), G_{hh}(r_k), G_{dd}(r_k)\}$, where M is four times the number of mesh points used for the radial integrations. Some initial guess G_j^0 enables us then to use the Newton-Raphson iteration[27] for the nonlinear system (61),

$$G_j^{m+1} = G_j^m - \sum_i \left(\frac{\partial X_i}{\partial G_j}\bigg|_{G^m} \right)^{-1} X_i(G^m). \tag{62}$$

The coefficient matrix, $\partial X/\partial G$, the linearization of the FHNC equations at G^m, is obtained in closed form from (17) and (18).

Usually 4 to 6 iterations of (62) are sufficient for a five-digit accuracy in the $G_{xy}(r_i)$. The only remaining problem is to choose the initial guess G^0 such that the iteration (62) converges. This is accomplished by solving the FHNC problem at low densities first and then increasing the density in sufficiently small steps. The solution corresponding to a lower density is then rescaled according to r_0 and used as initial guess for the higher density, a procedure well known in this context.[15]

One might ask why we do not use a much simpler iteration scheme. For example, with some initial guess G^0 one could evaluate (18), solve the linear systems (17), and iterate back and forth between (18) and (17). Unfortunately, this procedure converges only for very "easy" cases where the density is low or the CFN short ranged. In other cases the convergence is either extremely slow (one needs about 100 iterations in some cases) or nonexistent; the latter especially applies for ^{3}He.

Also one might try to solve the linear systems (17) by iteration as well. This procedure, however, breaks down even much earlier than the iteration between (17) and (18). As we enter here into the discussion of the physical significance of various terms, e.g., the permutation expansion for the antisymmetric wave function, this discussion will be deferred to the next section.

D. Evaluation of elementary diagrams

As was pointed out in Sec. II C, in order to execute the FHNC/4 approximation it is necessary to evaluate six-dimensional integrals of the basic structure shown in Figs. 4a, 6, 13, 15, and 18. All these diagrams are evaluated as functions of the distance between the two bottom points. There remains then a five-dimensional integral, namely over the radial distances and polar angles of the two field points with respect to one of the bottom points, and the azimuthal angle between the two field points. The latter integration is independent of the distance between the two external points such that in effect one has to perform only a five-dimensional integral to completely evaluate the energy contribution of a given diagram. These integrals are again evaluated using Gaussian integration on the same radial mesh as outlined in Sec. III B. The integrations over the polar angles are done on a 12-point Gaussian mesh which was found to be sufficient for a 5% accuracy in the FHNC/4 contributions despite the fact that one disregards the discontinuities in some higher-order derivatives for three of the six involved bonds. One may view the Gaussian integration in these cases as performing some implicit "smoothing" in the vicinity of the special points $r = r_c, d$. The innermost loop will perform the integration over the azimuthal angle between the two field points. The value of the radial distance between these points depends on all five integration variables. The bond function is given only on the mesh points, Sec. III B, however. So one has to perform some interpolation within the innermost program loop, unfortunately. A huge savings of computing time is gained by first interpolating the bond function between the two field points to a very closely spaced half-logarithmic table outside any integration loop by use of some higher-order formula, and then doing only linear interpolation within the integration loops. Another factor-of-3 savings is gained by taking the abscissae of the half-logarithmic table to be those corresponding to the

first 16 bits of the internal representation of a floating-point number used in the IBM/370 computer system. In that way the first 16 bits of the argument value where the function value should be computed can be taken as an index to the interpolation table, and no complicated table-lookup procedure involving divisions, etc. is needed.

That considerations of this kind are important is due to the large number of integrals (35 per iteration, and 99 per energy evaluation) needed. Whereas a FHNC-type calculation takes only about 20 sec on an IBM370/195, the FHNC/4-type calculation employing the optimizations sketched above uses about 20 CPU min per density such that a factor of 3 results in considerable savings.

IV. APPLICATIONS

A. Liquid ^{3}He

The classic example of a fermion liquid with short-range interaction is the ^{3}He liquid interacting via the Lennard-Jones potential

$$v(r) = 4\epsilon[(\sigma/r)^{12} - (\sigma/r)^6], \tag{63}$$

with the parameters $\sigma = 2.556$ Å and $\epsilon = 10.22$ °K. There are several earlier results to compare with. Schiff and Verlet[28] (SV) used a molecular-dynamics method to treat the ^{3}He Bose liquid and employed a permutation expansion, the Wu-Feenberg expansion,[29] to account for the antisymmetric wave function. They used a correlation factor of the form

$$f(r) = \exp[-\tfrac{1}{2}(b\sigma/r)^5], \tag{64}$$

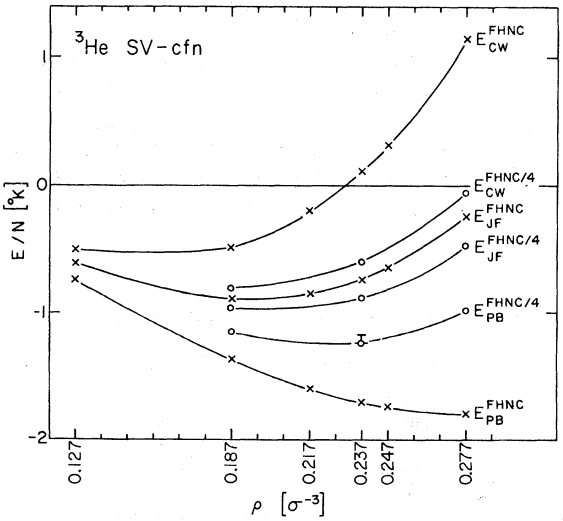

FIG. 19. Variational energies for ^{3}He using the correlation functions of Schiff and Verlet (Ref. 28). The error bar indicates the Monte Carlo result.

with the parameter $b = 1.13$ found to be optimal, i.e., minimizing (4). They obtained a saturation point at a density of $0.237\sigma^{-3}$ with an energy per particle of -1.35 °K. The same correlation function was used by Ceperley, Chester, and Kalos in their Fermi–Monte Carlo (MC) evaluation[9] of (4) at said density. They found the energy to be -1.20 ± 0.03 °K. In order to compare their results with ours, we also used the SV CFN (64) to evaluate the expectation value (4). However, in order to check on the convergence of the FHNC expansion, we used the three forms of KE defined in Sec. II D. The results are shown in Fig. 19. At low densities there is fair agreement between the different forms of KE, whereas at higher densities the uncertainty in the energy is embarrassing. As a consequence of this behavior, the three different forms of KE predict radically different saturation points; for the PB prescription there is no saturation at all within the density range studied. The PB form of the energy lies below all other results, whereas the other forms of KE lie considerably above the results of the MC evaluation. Clearly, in FHNC the RDF's are so uncertain at the interesting densities that it is very difficult to draw any conclusion from these curves regarding the energy of ^{3}He. It is possible to improve on these results, however, by taking into account the next order in the basic diagram expansion, i.e., to use the FHNC/4 approximation. For that approximation the different curves are much closer to one another, and for the PB prescription the saturation point coincides with the MC result. As the MC result is to be viewed as the upper bound corresponding to the correlation factor (64), it is seen that in FHNC the PB evaluation of the energy *does not constitute an upper bound* but lies considerably-about 20–40%-below the actual upper bound corresponding to the chosen wave function. The saturation density is estimated to be about the same amount too high. In FHNC/4, on the other hand, the PB prescription seems to give the most accurate result.

Before we discuss how the various terms in the energies affect these findings, let us report some additional calculations done with the PB-type CFN's defined via (50) and (51). The range of the CFN d was varied to obtain the minimum of the energy uniformly for all densities at $d = 2.4r_0$. As observed earlier,[15] the energy is quite insensitive to the value of d if d becomes greater than $2r_0$. Again the energy is evaluated using different forms of KE. The results are shown in Fig. 20. Qualitatively, the behavior is the same as for the SV CFN; however the differences between the different KE forms are generally smaller. This is mainly due to the smaller range of the PB CFN.

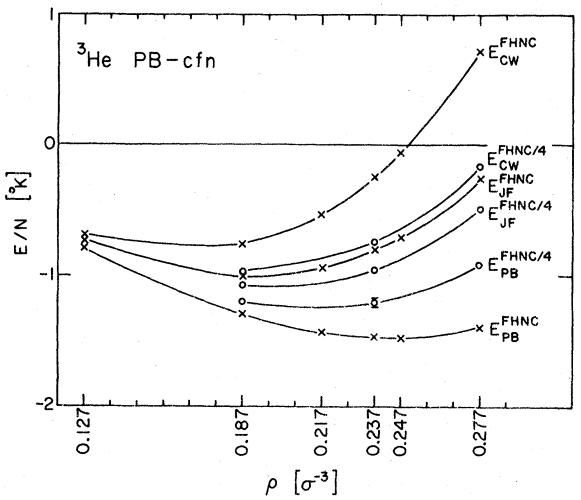

FIG. 20. Variational energies for ^{3}He using the correlation functions from Eq. (50). The error bar indicates the Monte Carlo result.

The parameter κ, Eq. (53), is for the SV CFN always about 1.3 times as large as for the PB CFN, ranging from 0.35 for the lowest to 0.85 for the highest density (SV CFN). The same CFN's (but with $d = 2r_0$, which should not make much difference) were used by PB.[15] They treated the ^{3}He Bose fluid via HNC/4, and also used a permutation expansion to deal with the Pauli exclusion principle. They found saturation at a density of $0.247\sigma^{-3}$ with an energy of -1.35 °K. It is seen that in both cases, SV as well as PB, the permutation expansion does quite well and is only about 10% off the MC result.

In Table I we give our FHNC/4 energies with the PB prescription for the KE for both choices of CFN together with the corresponding κ values. The last column gives the energies calculated by PB. These are in surprisingly close agreement with our FHNC/4 results. While this agreement seems to indicate that the permutation expansion is quite accurate, one has to be quite careful in that respect as will be clarified below. Comparing our results for the SV and PB CFN's, several remarks are due. Employing the PB form for the KE, there is in FHNC some energy gain going from the PB to the longer ranged SV CFN. One could conclude that this indicates that the SV CFN is "better" in the variational sense. This conclusion is just wrong, however, as in FHNC/4 both CFN's give almost identical energies and saturation densities. Also one would conclude using the SV CFN that the saturation density should be much higher than $0.237\sigma^{-3}$. As indicated by the FHNC/4 result, this would also be a wrong conclusion. This already indicates that employing the PB form of KE in the FHNC approximation might be quite misleading. This conclusion will be substantiated in the following sections.

Another conclusion is that the form of the correlation factor $f(r)$ does not matter very much, as was also observed in the Bose case. Though the SV and PB CFN's are quite different, a careful evaluation of the energy expectation value yields almost identical results. This substantiates our belief that it is not very important to optimize f carefully.

As another means to estimate the convergence of the basic diagram expansion, we proposed using the model KE; see Sec. II E. In Fig. 21 we show the model KE for the SV as well as the PB CFN's in FHNC and FHNC/4. As we expect from the preceding discussion, the FHNC model KE is for the SV CFN farther off the correct value T_ϕ than for the shorter-ranged PB CFN with its smaller κ value. With increasing density the FHNC model KE's get dramatically worse even changing the sign of the slope, i.e., giving less KE for increasing density. Employing the FHNC/4 approximation the agreement with the exact value T_ϕ is much improved, and the slope retains its correct (positive) sign. All this leads to the conclusion that in any given approximation one cannot trust just one evaluation of the energy, but must employ additional means in order to estimate the accuracy of the so-obtained results. Figures 19–21 show quite clearly that such estimates may be obtained from

TABLE I. FHNC/4 energies and wound parameters for ^{3}He. U_{PB} includes the ΔU corrections.

	SV CFN					PB CFN					PB[a]
ρ (σ^{-3})	κ	ΔU	U_{PB}	E_{PB}	E_{mod}	κ	ΔU	U_{PB}	E_{PB}	E_{mod}	E_{PB}
			(°K)					(°K)			(°K)
0.187	0.54	0.19	1.34	−1.15	−2.13	0.42	0.08	0.80	−1.20	−0.86	−1.21
0.237	0.71	0.44	2.61	−1.23	−2.20	0.56	0.25	1.67	−1.21	−0.33	−1.35
0.277	0.85	0.79	4.16	−0.98	−1.84	0.67	0.50	2.73	−0.91	+0.61	−1.27

[a] Reference 15.

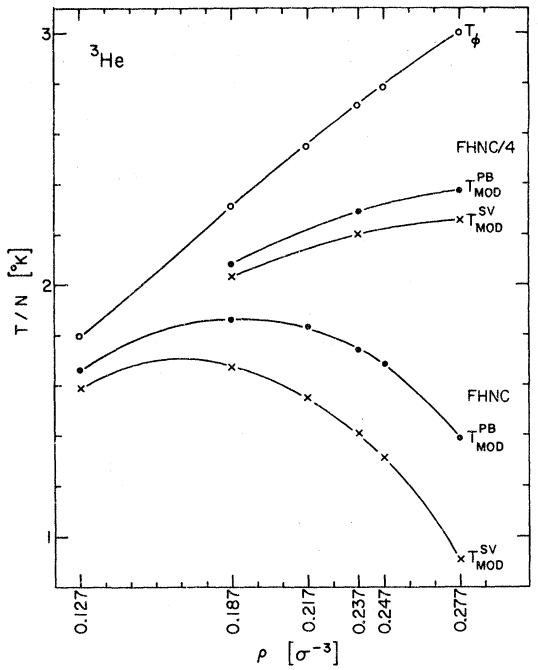

FIG. 21. Model kinetic energies for ^{3}He.

the different forms of KE.

All these findings may be understood with reference to the problems and advantages of the different KE forms, Sec. II D. As is well known, in FHNC approximation the two-body RDF is slightly too large for small distances. Since in the JF and CW prescriptions the core of the potential is retained to some degree within the "effective Hamiltonian" w_2, the FHNC version of these energies is too repulsive. Taking into account the four-point basic diagrams, i.e., E_{xy} in Eqs. (17)–(19), corrects $g(r)$ to some degree and thus results in some attraction for the JF and CW energies, whereas the PB energy remains almost unchanged. This observation, based on the two-body terms in the different KE prescriptions, led to the conjecture that the PB form is the most accurate. However, we should not forget about the three-body KE terms. In the JF prescription the three-body term W_{x3} is extremely small and does not matter for the discussion here. In the PB form we have, however, the large U term. As mentioned in Sec. II C, there is a direct contribution from the four-point basic diagrams to the three-body RDF and thus to U and U_F, Figs. 6 and 18. This contribution to U is called ΔU. The contribution to U_F again is small and does not matter here.

In Table I we give the values for U and ΔU. It is seen that with increasing density these terms rapidly increase. Also, in going from the PB to the longer-ranged SV CFN, these terms greatly increase. This is the behavior one would expect by just looking at the diagrams, Figs. 6, 18, and 11. Almost all the difference between FHNC and FHNC/4 for the PB form of KE is made up by this ΔU term. As the same term enters the CW form of KE with the reversed sign, the large change in the CW energy is explained: here the modification of $g(r)$ and ΔU are both attractive, whereas for the JF form there is no ΔU due to the smallness of the three-body term (we did not try to calculate this correction which would be much smaller than the numerical noise). For the model kinetic energy also the main repulsive contribution in going from FHNC to FHNC/4 comes from the ΔU term. It is thus to be stated that in the truncation of the expansion (10) applied to the energy attractive terms are omitted in the case of the JF or CW energies, which thus retain the upper-boundary property, whereas in the PB case repulsive terms are omitted. It follows that the PB energy in FHNC does not constitute an upper bound, though in FHNC/4 it might be an accurate estimate.

The relative sizes of U_{PB} and ΔU, Table I, may furnish another error estimate in FHNC. ΔU is generally about 10–20% of U_{PB}. ΔU is by far the leading correction to the PB energy. In FHNC one may therefore use an estimate of 10–20% of U_{PB} to improve on the PB energy, and obtain an error estimate of the same order.

Some remarks as to the convergence of the different iteration schemes involved are appropriate. In FHNC there is only one iteration involved, namely (62), in solving the system of nonlinear coupled integral equations (17) and (18). As mentioned in Sec. III C only a few iterations are needed, but the initial guess must be obtained from some results at lower density. It is possible to start at a density of $0.127\sigma^{-3}$ and increase the density in steps of $0.03\sigma^{-3}$. It is *not* possible to use the simple scheme of iterating (17) with (18) which we found to diverge at all densities considered here. In the non-self-consistent FHNC/4 scheme, one just has to solve (17) and (18) a second time after evaluating $E(r)$ from the first solution. In going to the self-consistent version of the FHNC/4 approximation an additional iteration is involved, namely, solving the FHNC equations for fixed E_{xy}, and calculating E_{xy} from the previous FHNC solution. At low densities, i.e., for the first two lines of Table I, already the second iteration affects the energies only by one or two digits in the last place given. For the higher density, $0.277\sigma^{-3}$, this iteration diverges however for the long-ranged SV CFN. (Observe that the convergence factor should be proportional to ρ^3 explaining this quite rapid change in behavior with increasing density.) This is *not* to be taken as indication of some seri-

ous trouple. As was the case for the FHNC iteration, (17) and (18), this is only a property of the special iteration path selection, and indicates that one should use a different means of solving the nonlinear problem. This was achieved for the FHNC equations by using the iteration prescription (62). Geometrically speaking, in order to linearize some function one should use the tangent, as done in (62), and not some arbitrary secant, as done in the case of the simple iteration of (17) with (18), or the iteration for the basic diagrams. In other words, one tries to sum a divergent geometric series by iteration, which is not possible. The first iterate is the most accurate estimate to the sum, however. Also it is not clear if one should perform the self-consistency iteration at all, regarding the higher-order terms omitted anyway in FHNC/4 approximation.

These observations, as well as the fast convergence of the basic diagram iteration for lower densities, led us to use the following prescription in all of the FHNC/4 calculations reported here: After solution of the FHNC problem, evaluate *once* the sum of elementary diagrams E_{xy} corresponding to the four-point basic diagrams, and solve again the FHNC equations (17) and (18) with these E_{xy}, using again the iteration (62). With the resulting G_{xy} and the given E_{xy} we then evaluate the two- and three-body RDF's with inclusion of the explicit four-body terms in the three-body RDF, Figs. 6 and 18, which give rise to the ΔU term. In other words the iteration of the basic diagrams with the FHNC equations is not performed, but of course the superbonds (23) are used for the construction of the E_{xy}; i.e., diagrams like Figs 13–16 are included in our FHNC/4 scheme whereas diagrams like Fig. 17 are not.

The ΔU term is then evaluated from the 99 diagrams corresponding to the one Bose diagram Fig. 6(a), few of which are shown in Fig. 18 where again the S_{xy} bonds are used. This term has previously only been evaluated for bosons and was found to be relatively small, although it was the leading correction to HNC for the PB energy.[16] For fermions the complete ΔU is about five times as large as the contribution from Fig. 6 alone. This is due to a vast number of diagrams containing exchanges and having the same sign, e.g., there are 12 diagrams where one of the bonds in Fig. 6 is replaced by a S_{sh} bond, as shown for example in Fig. 18(d). It is this conspirative feature of the many diagrams containing exchanges which makes the ΔU so large for fermions and thus renders the PB form of KE inaccurate in the FHNC approximation, to about 10–20% of U_{PB}. The question of course remains what the effect of the many thousand FHNC/5 diagrams will be.

In Table I we also give the model energies defined in Sec. II E. These do not agree with the variational energies. For softer potentials than the Lennard-Jones potential there is much better agreement between variational and model energies;[6] see also the following subsections. We take this as an indication that, though the variational energies for the SV and PB CFN's are very close to one another, both of the corresponding wave functions are far from true eigenstates of the Hamiltonian (42).

The experimental result[30] for the energy is -2.52 °K and for the saturation density $0.274\sigma^{-3}$. Our variational results give much less binding energy and a lower saturation density. This should partly be due to the inadequate description of the actual Hamiltonian by the Lennard-Jones potential (63) which yields already in the Bose system more than 1 °K underbinding.[15,28] On the other hand, the disagreement between variational and model energies indicates an inadequacy of the two-body Jastrow wave function (2), i.e., three- or more-body correlation functions are important for ^{3}He.

This finding is substantiated by recent evaluations of three-body correlation contributions to the ^{4}He (bose) liquid energy,[42] which is found to be -0.3 °K for the densities of interest here. This quite large contribution is to be opposed to corresponding calculations for Yukawa potentials[32] which yield extremely small contributions. We conclude that three-body correlations are much more important for hard potentials than for soft ones, and that a large difference between model and variational energies is an indication for this importance.

B. Fermion homework problem

Several authors[21,31,9] have agreed to study the so-called fermion homework problem, a generalization of the original homework problem[32] for the Bose case. They consider a system of neutrons (obeying Fermi statistics) interacting via the potential

$$v(r) = 9263.1 \exp(-4.9r)/r \qquad (65)$$

with r in fm and v in MeV. In order to compare with these results we used the same potential and CFN's. The problem was proposed by Krotscheck and Takahashi (KT), who used an alternative FHNC method to be discussed below. They used a CFN of the form

$$f(r) = \exp[-\tfrac{1}{2}(b/r)e^{-r/b}], \qquad (66)$$

and the CW prescription for the KE. The same CFN's were used later by Fantoni and Rosati[31] (FR), who used the same FHNC method used here.

TABLE II. Model kinetic and variational energies for various correlation functions and approximations for the fermion-"Homework" problem.

Fermion-homework $s=2$																														
ρ (fm^{-3})	Method	MC	KT E_{CW}	FR E_{JF}	KT CFN κ	KT CFN E_{CW}	KT CFN E_{JF}	KT CFN E_{PB}	MC CFN κ	MC CFN E_{CW}	MC CFN E_{JF}	MC CFN E_{PB}	PB CFN $d=2r_0$ κ	PB CFN $d=2r_0$ E_{CW}	PB CFN $d=2r_0$ E_{JF}	PB CFN $d=2r_0$ E_{PB}	PB CFN d/r_0	PB CFN κ	PB CFN E_{CW}	PB CFN E_{JF}	PB CFN E_{PB}	PB $d=2r_0$ T_ϕ	PB $d=2r_0$ T_{mod}	PB $d=2r_0$ E_{mod}	KT T_{mod}	KT E_{mod}
0.17	FHNC	89							0.18	95	91	86	0.29	93	91	88						37	34	85		
	/4									91	90	89															
0.2	FHNC		108	112	1.11	115	112	108					0.31	112	109	105						41	37	102	38	119
0.3	FHNC	175							0.34	197	179	158	0.39	181	174	166	3.0	0.76	186	174	162	53	46	162		
	/4									178	177	176															
0.4	FHNC		238		2.00	265	255	244					0.46	257	247	234						65	54	229	56	269
0.6	FHNC		390	424	2.84	442	424	405					0.55	432	412	388	3.0	1.16	449	412	373	85	64	381	67	441
0.8	FHNC		560		3.55	641	614	585					0.62	629	598	562						103	71	554	75	633
1.0	FHNC	732	744	824	4.35	858	819	778	1.33	835	795	751	0.68	844	802	753	3.0	1.55	882	805	720	119	77	743	79	834
	/4					808	811	811		793	790	787		811	798	782											
1.2	FHNC		941		5.01	1090	1039	985					0.73	1076	1022	958						134	80	947	80	152
1.4	FHNC		1149	1285	5.42	1335	1274	1208					0.76	1321	1254	1177	2.8	1.61	1387	1258	1118	149	83	1163		
	/4					1262	1262	1256						1268	1248	1223											
1.6	FHNC		1366										0.80	1577	1448	1406						163	84	1391		
2.0	FHNC	1976							2.52	2128	1994	1847	0.85	2119	2014	1894	2.6	1.60	2219	2023	1809	189	86	1875		
	/4													2037	2006	1967											

FR use the JF form of KE. Also there are Fermi-Monte-Carlo[9] (MC) results available. These were obtained using a different form for the CFN

$$f(r) = \exp[-(A/r)e^{-Br}(1 - e^{-r/D})]. \tag{67}$$

For the sake of comparison all these results are given in Table II together with our results. First we used the CFN (66) with the parameters b as given by KT and used also by FR. For the JF choice of KE our results agree to within the numerical accuracy of 1% with those obtained by FR using the same prescription. The KT results obtained from the same CFN with the CW prescription for the KE are consistently below all three results obtained by us in FHNC. The spread between the different KE prescriptions is only 10% or less in FHNC in spite of the quite large κ values. Employing the FHNC/4-approximation results in a remarkable improvement making all energies equal to within numerical accuracy. We thus believe that this converged value is the true upper bound corresponding to the CFN (66). The KT results are, however, 10% below these energies and thus underestimate the upper bound.

In order to compare with the MC results, we used also the CFN (67). Again the different FHNC energies differ by only 10% at most, and in FHNC/4 remarkable agreement with the MC result is achieved over the entire density range. This substantiates our belief expressed in the last subsection that in FHNC/4 quite an accurate estimate for the variational upper bound is obtained, and that the difference between the different forms of KE is a good measure for this accuracy.

In addition to the CFN's (66) and (67), we also used the PB CFN's obtained from (50) and (51) with a fixed $d = 2r_0$. The energies are not much different from those obtained with the CFN (67). Both these energies are, however, somewhat below the energies obtained with the CFN (66) indicating that the one-parameter form (66) is not sufficiently flexible. However, whether one uses three parameters, as in (67), or solves the differential equations (50) and (51) seems to make little difference, confirming again that the details of the CFN do not matter as long as one is within some reasonable range of CFN's. The last columns of Table II give the model kinetic energies and model energies for the KT and PB CFN's. It is seen again that the difference between the model KE and its exact value T_ϕ provides a good measure for the accuracy of FHNC. The model energies are quite close to the variational energies such that we cannot conclude that the chosen wave functions are far from the ground-state wave function (42). Because of the smallness of corrections due to three-body correlations in the corresponding Bose li-

quid,[32] we conclude that the variational wave function is indeed close to the true ground-state wave function.

In summary, Table II demonstrates that one is able to obtain estimates for an upper bound by means of the FHNC approximation within the uncertainty given by the various forms of KE. In FHNC/4 then an accurate estimate to the upper bound is obtained.

We warn the reader, however, that one *cannot* say in general that FHNC always gives a reasonable estimate to the upper bound if just one form of the KE is used. It is necessary in FHNC to constrain the CFN to be of not too long range if the PB or CW prescriptions for the KE are used. This is exemplified in Fig. 22 where for fixed density $\rho = 1$ fm^{-3} the range of the PB CFN, d, is varied. It is seen that for small d the convergence of FHNC is good, but the upper bound comes out quite high as the CFN is restricted too much. With increasing d, all energies come down, but differ more and more from one another such that the accuracy of the results becomes doubtful. Increasing d beyond $2r_0$ results in the PB energy still decreasing, whereas the JF energy exhibits a minimum and the CW energy rises quite high again. This leads to the conclusion that in FHNC it might be very dangerous to use the PB prescription for the KE blindly as one might underestimate the upper bound significantly. That this is due to the bad convergence of the basic diagram expansion for long-ranged CFN's is shown by the dramatic improvement obtained by using the FHNC/4 approximation. Then for all KE forms the minimum of the energy occurs at the same range, $d = 2r_0$, and for the PB form coincides with the MC result. However, despite the small difference between FHNC and FHNC/4 for the JF energy the contributions from the elementary diagrams, E_{xy} in (17) and (18) become so large for $d = 2.8r_0$ that we could not find a solution to the nonlinear system (17) and (18). The values given for FHNC/4 in that case consist just of the FHNC values plus the ΔU (and ΔU_F for E_{PB}) contributions evaluated from the FHNC G_{xy}. This indicates that one has to exercise some care in going to long-ranged CFN's and high densities.

The last statement is emphasized even more by the FHNC results given in Table II for PB CFN's where the PB energy is minimized for d. This energy-density curve deviates significantly from the upper bounds obtained with the more reliable methods. With increasing density there is a spurious gain in energy due to the higher-order contributions omitted. All the deviations discussed here are about 10% of the total energy for this example. This might look like quite a small number indicating that any method is reliable within 10%. One must, however, take into account that for this example there is no cancellation between potential and kinetic energy as both are positive. This leads to a better relative accuracy than for attractive forces. The absolute numbers might give a better impression of the accuracy: at nuclear matter density the error is about 8 MeV, and increases to more than 100 MeV for higher density.

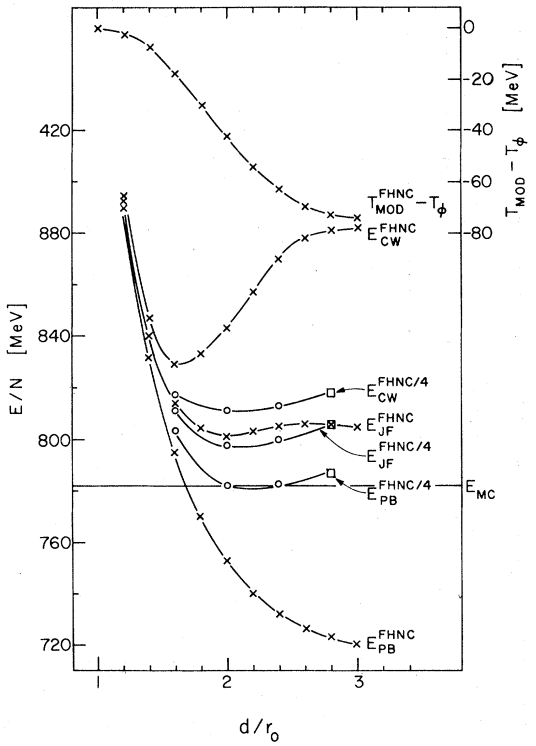

FIG. 22. Model kinetic and variational energies for "homework" neutrons at a density of 1 fm^{-3} as function of d/r_0.

A puzzling feature about the different CFN's used is that despite the large values for κ, Eq. (53), in the case of the KT CFN (66) the deviations between the different forms of KE remain comparatively small. This must be regarded as a special property of the functional form (66), since for increasing κ in the case of the PB CFN, the energies do deviate increasingly from one another.

In Fig. 22 the topmost curve shows the deviation of the model KE from its exact value T_ϕ, in FHNC approximation. As expected this difference behaves similarly to the difference in the variational energies and constitutes a good measure for the truncation error of the basic-diagram expansion.

TABLE III. Model and variational energies for the potential v_2 for both degeneracies, $s=2$ (neutrons) and $s=4$ (nuclear matter). U_{PB} includes ΔU. Energies in MeV.

	ρ (fm^{-3})	E_{MC}	FHNC E_{CW}	FHNC E_{JF}	FHNC E_{PB}	FHNC/4 E_{CW}	FHNC/4 E_{JF}	FHNC/4 E_{PB}	FHNC/4 U_{PB}	FHNC/4 ΔU	FHNC T_ϕ	FHNC T_{mod}	FHNC E_{mod}	FHNC/4 T_{mod}	FHNC/4 E_{mod}	FHNC/4 ΔU
$s=2$	0.182	12.0±0.4	14.7	13.6	12.4	13.8	13.2	12.9	5.0	0.56	38.2	37.3	11.3	37.8	11.7	0.44
	0.386	17.3±0.1	26.8	19.7	11.7	20.0	18.0	16.7	29.3	4.67	63.1	56.0	−0.2	60.6	3.8	3.7
	0.822	60.0±2	98.4	75.0	48.3	77.5	71.6	64.9	89.9	15.7	104.5	79.6	30.9	97.2	46.0	13.7
$s=4$	0.182	1.9±0.5	4.8	4.1	3.2	4.1	3.8	3.5	5.2	0.26	24.1	23.5	4.1	23.9	4.3	0.2
	0.386	3.4±0.5	12.4	7.6	2.1	8.1	6.4	4.4	29.4	2.29	39.8	34.8	−7.6	37.9	−5.5	1.9
	0.822	54.5±0.5	77.4	61.5	43.8	63.4	58.0	51.5	90.5	7.92	65.8	49.3	33.3	59.8	40.6	6.8

C. Potential v_2

A very useful test potential is

$$v_2(r)=[9924.3\exp(-4.2r)-3187.8\exp(-2.8r)+105.468\exp(-1.4r)-10.463\exp(0.7r)]/(0.7r)\,, \quad (68)$$

which is the central part of the Reid $^3S_1$-$^3D_1$ potential[10] assumed to act in all partial waves. This potential was first used by Pandharipande, Wiringa, and Day,[7] and subsequently by other authors,[33,6] including Ceperley, Chester, and Kalos.[9] In order to compare with the latter's MC results, we used their CFN's which are of the form (67). For both degeneracies, $s=2$ (neutron gas) and $s=4$ (nuclear matter), results of FHNC and FHNC/4 calculations are given in Table III. All these results essentially confirm the findings in the previous subsections. With increasing density in FHNC the different forms for the energy yield diverging results which may be made less divergent by using the FHNC/4 approximation. The model kinetic energy exhibits the same behavior with respect to its divergence from the exact value T_ϕ. The FHNC/4 results agree quite well with the MC results except for the two lower densities in the nuclear matter case ($s=4$) where they come out slightly above the MC values. One has to bear in mind, however, that these extremely small numbers result from a cancellation of about −100 MeV of potential energy against a similar amount of kinetic energy, so that any results for these cases are inherently inaccurate. Our numerical accuracy is better than 0.5 MeV. However, our calculation differs slightly from the MC calculation as no "smoothing" of the CFN was performed and also in that there are no finite size effects in our calculation. In addition there are still some contributions to be expected from FHNC/5.

Again it may be seen from Table III that the ΔU correction is about 10% of U_{PB}. As this seems to be a fairly constant relation, one would again suggest that in FHNC calculations using the PB prescription for KE, 10% of U_{PB} could be used as approximate correction and error estimate.

For comparison we give results of a lowest-order "Brueckner" calculation with standard dispersion (LOBT) as obtained by Day[34] in Table IV. The last column gives κV which is a reasonable estimate of the uncertainty in a calculation not including three-body clusters. It is seen in comparison with Table III that the discrepancy to the variational results is much less than κV so that it is perfectly reasonable to expect results below the variational energies if the three-body cluster is included in the perturbation treatment.

TABLE IV. Lowest-order "Brueckner"-theory results for nuclear matter with potential v_2 as obtained by B. D. Day.

k_F (fm^{-1})	ρ (fm^{-3})	V (MeV)	T (MeV)	E (MeV)	κ	κV (MeV)
1.4	0.185	−19.7	24.4	4.7	0.140	−2.8
1.5	0.228	−22.8	28.0	5.2	0.167	−3.8
1.6	0.277	−25.7	31.8	6.1	0.198	−5.1
1.7	0.332	−28.4	35.4	7.5	0.232	−6.6
1.8	0.394	−30.5	40.3	9.8	0.270	−8.2
1.9	0.463	−32.1	44.9	12.8	0.314	−10.1
2.0	0.540	−32.9	49.8	16.9	0.363	−11.9

V. DISCUSSION AND CONCLUSIONS

A. Antisymmetry

In the preceding section it has been demonstrated that by using the FHNC and FHNC/4 approximations, a converging energy is obtained by evidence of the various checks employed. This energy coincides or is in reasonable agreement with Fermi-MC calculations. As the latter treat the wave-function antisymmetry correctly beyond doubt, it follows that at least for the energy the FHNC treatment of antisymmetry, i.e., expansion in powers of $-1/s$ and doing the indicated partial summations on this expansion, is sufficiently accurate. As the different forms of KE tend to agree in FHNC/4, however, we conclude that also the

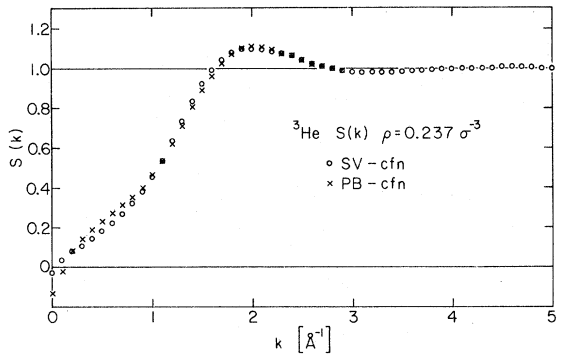

FIG. 23. Liquid-structure functions for ^{3}He.

radial distribution function cannot be very wrong for the relevant distances. Thus the only possible place where some trouble may arise is the long-range part of the RDF.

It is useful to introduce the liquid structure function $S(k)$, the Fourier transform of the two-body RDF,

$$S(k)=\rho\int d^3\vec{r}\,[g(r)-1]e^{i\vec{k}\cdot\vec{r}}+1\,. \tag{69}$$

In order to test the long-range behavior of $g(r)$, we are then interested in the small-k behavior of $S(k)$. It is a well-known result[14] that for small k, $S(k)$ is linear in k, $S(k)=\text{const}\times k$. In particular, we have the normalization condition $S(0)=0$, which may alternatively be written as

$$S(0)=\rho\int d^3\vec{r}\,[g(r)-g_F(r)]=0\,. \tag{70}$$

It is seen that the long-range behavior of $g(r)$ enters into this condition with a large weight. In Fig. 23 we show the liquid-structure functions for ^{3}He at a density of $0.237\sigma^{-3}$ for the two CFN's considered, calculated in the FHNC approximation. The FHNC/4 approximation does not differ perceptibly in this plot. The normalization condition (70) is not quite met. However, the value of $S(0)$ strongly depends on the mesh used for the numerical calculation, and especially on the cutoff $R_{\max}$ discussed in Sec. III B. By changing the mesh one may easily vary $S(0)$ between +0.1 and −0.1, and one would have to use a much larger number of mesh points together with a much larger $R_{\max}$ than $20r_0$ in order to pin down this number. Fortunately, the energy and all other quantities calculated do not depend on this long-range part of $g(r)$. As soon as one reaches moderate values of k, about 0.2 Å^{-1}, which is about the region where the experimental results[35] begin and is thus sufficient for comparison with experiment, the liquid-structure function becomes quite stable against variations in $R_{\max}$. However, as in earlier variational calculations using the Lennard-Jones potential,[28] the calculated energy and saturation density are quite far from the experimental values so that a comparison is not very meaningful. We arrive thus at the conclusion that for any practical purpose the FHNC or FHNC/4 evaluation as described here is sufficient and correctly treats the wave-function antisymmetry.

It has been conjectured[36] that methods employing permutation expansions to treat antisymmetry, i.e., expansions in powers of $-l/s$, treat antisymmetry incorrectly and may exhibit spurious or bad convergence properties. This is indeed true for straightforward permutation expansions, i.e., *not* using partial summations. For the case of low densities and short-ranged CFN's such an expansion converges, whereas for higher densities it diverges. Table V shows some results obtained with the potential v_2 at densities of 0.1 and 0.386 fm^{-3}, using the CFN (67) with the parameters for the higher density in both cases. After solution of the Bose-HNC equations (13), for G_{ss}, the linear integral equations (17) were iterated, generating the chain-type diagrams Fig. 8–10, for the $G_{sh,\,hh,\,dd}$ functions, where the solid line denotes the Bose $g(r)-1$ bond. The linear terms in (19) for the $G_{sh,\,hh,\,dd}$ functions were used to calculate contributions to the JF two-body energy (24) and (32). Table V shows the contributions from different orders in these iterations. For the lower density all iterations converge nicely, whereas for the higher density the *sh* and *hh* iterations diverge and only the *dd* iteration converges. This demonstrates that permutation expansions for antisymmetry generally are not converging unless partial summations are performed, as is done for example in any FHNC method. In sufficiently low order, however, the results of such an expansion are surprisingly accurate as evidenced by the earlier variational calculations for fermion liquids[15,28] which are generally only about 10% off in the energy. This is a behavior frequently observed with divergent series. Also, it is not surprising that even for a divergent expansion, partial summations are perfectly capable of producing the correct re-

TABLE V. Iteration of Fermi-chain diagrams for nuclear matter potential v_2 at low and high density (in MeV).

	$\rho=0.386$ fm^{-3}			$\rho=0.1$ fm^{-3}		
n	*sh*	*hh*	*dd*	*sh*	*hh*	*dd*
1	+6.13	−0.7	−0.63	−1.04	+0.20	+0.14
2	−12.98	+1.4	−0.16	+0.46	−0.10	+0.01
3	+24.3	−2.9	−0.03	−0.22	+0.05	0
4	−44.6	+5.8	0	+0.11	−0.02	0
5	+83.6	−11.6	0	−0.06	+0.01	0
6	−154	+23.1	0	+0.03	0	0

sult. The conclusion is that though heavy criticism may apply to any finite order of a permutation expansion, the partial summations included in FHNC are sufficient to overcome this problem.

The quite different behavior of the *sh*, *hh* iterations on the one side and the *dd* iteration on the other side, which is generally found in all iterations involved [e.g., (17) with (18), or the iterations to include the elementary diagrams], motivates our belief that the graphical notation of FR is better adapted to a quantitative treatment of FHNC problems. Series of diagrams involving *dd* bonds are generally small and converging, whereas series involving helical elements may be dangerous and need to be treated with care. This behavior may easily be understood as the dashed lines represent the function $-l/s$ which oscillates around zero, whereas the helical lines represent the function $-l^2/s$ which is negative everywhere, such that integrals involving the former generally will be small due to cancellation.

There exists an alternative FHNC method[5] due to Krotscheck and Ristig (KR-FHNC) which differs from the method used here (FR-FHNC) in the partial summations performed on the permutation expansion of antisymmetry. It has been shown[37] that there exist certain exact cancellations, called Fermi cancellations, between various terms in this expansion. These are most pronounced for long-range CFN's and occur mainly for large distances, i.e., small values of k in the Fourier transforms of the various functions involved. In the FR-FHNC way of doing partial summations these cancellations are ignored in the sense that for terms included in a FR-FHNC/n approximation there are cancelling terms in higher orders, e.g., FR-FHNC/$n+1$. More specifically, the long-range part of some FR-FHNC contributions is exactly cancelled by some FR-FHNC/4 contributions, and so on. One could thus believe that the FR-FHNC expansion in terms of n-point basic diagrams converges badly, and that there exists some different ordering scheme (KR-FHNC) which would yield better convergence. Unfortunately, for KR-FHNC only the CW energies are available, and there have not been performed any of the tests using other forms for the KE, or calculating the error in the model KE. The reported KR-FHNC results[38,21] are in reasonable agreement with the FR-FHNC results for ^{3}He, but somewhat low for the fermion-homework problem, Table II. It is hard to believe that the variational energy obtained with the one-parameter CFN (66) used by Krotscheck and Takahashi should be below those obtained with a three-parameter form (67), used in the MC calculation; i.e., we should have $E_{\text{KR-FHNC}} > E_{\text{MC}}$. The opposite holds true, however. We conclude therefore that in the KR-FHNC scheme the variational upper bound may be underestimated yielding too attractive energies.

The KR-FHNC result is much farther off from E_{MC} (about 10%) than the difference between the various FR-FHNC/4 energies for the same CFN, which indeed lie above the MC energy. The KR-FHNC calculation does involve, however, already four-point elementary diagrams, and on the next level of sophistication one would have to evaluate five-body basic diagrams. We thus conclude that on the four-body level FR-FHNC provides a more accurate evaluation of the energy than KR-FHNC even for the long-ranged CFN's (66) used in this case, though FR-FHNC disregards the so-called "Fermi cancellations." This observation, together with the fact that the energy expectation value is quite insensitive to the long-range behavior of the RDF, nourishes the belief that these cancellations might not be as relevant as suggested. Indeed it might be much more important to accurately describe the *short-range* behavior of the RDF, and to this end it might very well be worthwhile to disregard the "Fermi cancellations." In other words, typically there are two contributions $A+B$ which will be kept together in the KR-FHNC approach because they cancel exactly in the low-k limit. In the FR-FHNC approach, A will be taken along whereas B will be discarded in a given approximation, because A is of FHNC or FHNC/4 type, but B is a five-point basic diagram. The numerical results seem to indicate now that for the relevant momenta (or distances) involved in the energy-evaluation, B is much smaller than A, and one should adhere to the FR-FHNC scheme. Then one might get a bad approximation for the long-range behavior of the RDF, but an accurate energy.

Moreover, our results indicate that not much energy is gained using long-ranged CFN's. It is thus perfectly reasonable to restrict the range of the CFN in some way. A practical way to do so is to use the PB form (50) and (51) and minimize for d in the FR-FHNC/4 approximation which yields $d=2r_0$ for all cases studied so far. In this way one may avoid the problem of long-ranged CFN's, and the corresponding convergence problems, in order to obtain a reliable upper bound together with the error estimates provided by the different forms for the KE. In the case of short-ranged CFN's, however, the expansion in terms of number of points in basic diagrams converges well.

Another troublesome point in the KR-FHNC approach is that after obtaining the liquid-structure function $S(k)$ carefully observing the "Fermi cancellations," some additional diagrams are added[37,38] in order to get a reasonable $g(r)$ for small r. This already indicates that the short-range parts of the

problem might not be dealt with very well in the KR-FHNC method. The relation between $g(r)$ and $S(k)$, Eq. (69), does not hold here. If one evaluates $g(r)$ by inversion of (69) in the KR-FHNC method, it will turn out to be unreasonably large for small r. After adding the diagrams to correct for this, one could of course use (69) again to get a modified $S(k)$. This function would, however, violate the conditions used earlier to derive the approximation scheme. In effect, different approximation schemes are used for evaluation of $g(r)$ and the energy on the one hand and for solving the KR-FHNC equations and evaluating $S(k)$ on the other. In the FR-FHNC approach one aims consistently at obtaining a reasonable $g(r)$ in order to evaluate a reasonable energy, whereas $S(k)$ then follows from (69) and might be badly described for small k. In a variational method, however, the minimum of the energy determines the wave function to be used, and it is therefore quite important to describe the *energy* properly in order to obtain a reasonable wave function.

To summarize this subsection, we do not see any strong arguments forcing one to deviate from the FR-FHNC scheme. It would, however, be extremely interesting to apply the convergence checks developed in this paper to the KR-FHNC method as on a sufficient level of sophistication both methods should agree, i.e., on any level the error bands expressed in terms of the various KE's should overlap.

B. State-dependent correlation functions

It has been suggested[15] that instead of using the state-independent CFN's defined by (50) and (51), one use solutions of the differential equation

$$\left[-\frac{\hbar^2}{m}\left(\frac{d^2}{dr^2}-\frac{l(l+1)}{r^2}\right)+v(r)\right]u_{lk}(r) = \left(\frac{\hbar^2}{m}k^2+\lambda_{lk}\right)u_{lk}(r), \qquad (71)$$

with the boundary condition

$$\frac{d}{dr}\ln u_{lk}(r)\Big|_{r=d} = \frac{d}{dr}\ln[j_l(kr)kr]\Big|_{r=d}. \qquad (72)$$

A state-dependent CFN f_{lk} is then defined by

$$f_{lk}(r)j_l(kr)kr = u_{lk}(r); \qquad (73)$$

i.e., in each partial wave different CFN's are to be used. Obviously, the FHNC equations as given in (17) and (18) cannot accommodate this complication as the CFN is assumed to be the same in all partial waves. If one wants to use the CFN's (73), one therefore has to derive a corresponding generalization of (17) and (18) first.[11] In some earlier calculations[15,7] an approximate treatment has been used which was subsequently criticized by the author.[6] It seems appropriate to clarify these remarks.

The approximate treatment of the CFN's (73) consists in defining an average CFN

$$f^2(r) = \frac{\int_0^1 dx\, n(x)\sum_l (2l+1)[1-(-)^l(1/s)]f^2_{lk}(r)j_l^2(kr)}{\int_0^1 dx\, n(x)\sum_l (2l+1)[1-(-)^l(1/s)]j_l^2(kr)}, \qquad (74)$$

where

$$n(x) = 24x^2(1-\tfrac{3}{2}x+\tfrac{1}{2}x^3), \quad k = xk_F. \qquad (75)$$

The denominator of (74) is equal to the free Fermi-gas RDF $g_F(r)$, Eq. (52). This average CFN is then used in solving the FHNC equations (17) and (18), and to evaluate a function $g(r)$, Eq. (19). The two-body part of the PB energy (see Sec. IID) is then approximated by

$$T^{(2)}_{\rm PB} + W_F = \tfrac{1}{2}\rho\int w(r)g(r)\,d^3\vec{r}, \qquad (76)$$

where $w(r)$ is given by

$$w(r) = v(r), \quad r>d,$$
$$= \frac{\int_0^1 dx\, n(x)\sum_l (2l+1)[1-(-)^l(1/s)]\lambda_{lk}f^2_{lk}(r)j_l^2(kr)}{f^2(r)g_F(r)}, \quad r\le d. \qquad (77)$$

Observe that the first part of (77) follows from the second if we put $\lambda_{lk}=v$ for $r>d$. The contribution W_F is *not* calculated from Eq. (29) but is part of $\lambda_{lk}f^2_{lk}j^2_l$ as may be seen from (71) and (73). For the three-body terms the average derivative is defined by

$$\frac{f'f}{f^2}(r) = \frac{\int_0^1 dx\, n(x)\sum_l (2l+1)[1-(-)^l(1/s)]f'_{lk}(r)f_{lk}(r)j_l^2(kr)}{f^2(r)g_F(r)}, \qquad (78)$$

so that (28) and (30) are easily evaluated.

Several comments apply to this approximate treatment. First, the CFN $f_{lk}(r)$ defined by (73) may have poles, as the zeros of u_{lk} need not coincide with the zeros of the Bessel functions. Second, consider the contribution W_F present in (76) and (77). Within W_F an exchange line is differentiated [the derivative operates on the j_l as part of u_{lk} in Eq. (71)] such that there are already exchange lines attached to the two external points of the W_F contribution to $w(r)$. In (76) however, this is multiplied by the full $g(r)$ again containing all possible exchanges on the two external points. In this way diagrams are calculated with as many as four exchange lines entering each of the two external points. Such diagrams clearly should not be present.

As the $v(r)$ part of λ_{lk} in (77) does not depend on l, k, it commutes with the averaging procedure. Thus the expectation value of the potential corresponds exactly to the correctly evaluated one using from the outset the state-independent CFN defined by (74) everywhere, i.e., in lowest as well as in higher orders. As the average CFN (74) is very close to the state-independent one, the potential energy remains almost unchanged by introducing state dependence. This is not true for the kinetic part in (77). This does not commute with the averaging procedure because different functions are differentiated. Here the CFN's used in lowest order and in higher orders really are different. The main problem seems to lie with the three-body kinetic energy U, calculated from the average derivative (78). The $f'f$ functions for the various l, k look quite different, and it is by no means clear that using the average is a good approximation especially as additional structure is brought in by the $\cos\theta$ resulting from the scalar product in (28). It is necessary to evaluate at least this three-body term exactly by using the partial-wave representation for all three bonds.

That indeed the kinetic energy is evaluated incorrectly is evidenced by Tables III and IV of Ref. 6. The model kinetic energies come out much too low; i.e., there is some spurious reduction of kinetic energy. Also the result depends strongly on the averaging procedure used, so that averaging is inherently inaccurate.

C. Summary

The main purpose of this paper has been to examine a specific variant of FHNC methods as to its convergence properties and to establish some measure of its accuracy. This goal has been achieved by evaluating the variational kinetic energy in three different ways. The differences between the three results which must vanish for an exact calculation furnish an error estimate for the energy evaluation. In addition, for the model kinetic energy, Eq. (45), we obtain directly the error due to the approximations made. Without doing any calculation going beyond FHNC, one may thus estimate the error due to omitting the elementary diagrams. Going beyond this type of calculation, it has been possible to take into account the elementary diagrams generated from the four-point basic diagrams, Figs. 13–18. This results in a significant improvement on the energies and saturation points. The change in the Pandharipande-Bethe form of the energy is generally about 10% of the three-body kinetic energy in the repulsive direction. This observation may be used to correct the PB energies if only a FHNC calculation is done, and furnishes an additional error estimate.

It has been shown in Sec. IV that for not-too-high densities and not-too-long-ranged correlations functions, reliable estimates to a variational upper bound to the energy may be obtained, but that some care needs to be exercised in going to higher densities and/or long-ranged correlation functions. In all cases studied the Clark-Westhaus and Jackson-Feenberg forms of kinetic energy result in the energy being an upper bound, whereas the Pandharipande-Bethe form may be too attractive. Arguments questioning the validity or accuracy of the treatment of wave-function antisymmetry do not apply to the present calculation, as evidenced by the numerical results. Therefore, we are content that within the indicated limits the present method is well suited to treat fermion liquids interacting via state-independent, local, central forces. In order to treat more complicated Hamiltonians, the method needs to be modified, however.

These findings put us in a position such that we are able to compare our method with other many-body methods. The alternative KR-FHNC method[5] does not seem to be at significant variance with the FR-FHNC method[4] as presented here. An independent convergence check employing the methods developed here would be extremely useful, however.

The comparison with lowest-order, i.e., two-body, "Brueckner"-type calculations using the Bethe-Brandow prescription for single-particle energies[3] shows agreement within reasonable estimates for the three- and four-body terms in one or other kind of linked-cluster expansion.[3,39] The two-body approximation comes out too repulsive, but the presumably attractive three-and four-body contributions (for an attractive potential) should make up for this. It is seen, however, that some over-optimistic estimates as to the convergence of linked-cluster expansions[3] based on some early, quite approximate estimates for the three- and four-body terms, might have been misleading.

Current interest in the nuclear matter problem is focussed on methods treating the full nuclear Hamiltonian, i.e., using for example the full Reid potential. For this case the three-hole-line term in hole-line classification scheme of linked clusters has been evaluated,[40] but there remains some uncertainty due to a lack of accurate evaluations of the four-hole-line part. The variational treatment[11,41] on the other hand also is not free of approximations, and we believe it to be especially troublesome that current calculations in the FHNC approximation lead into the range of high densities *and* long-ranged correlation functions. In order to establish these results to be actual upper bounds on the energy, it seems to be quite useful to employ at least some of the convergence checks outlined in this paper. Therefore, at the present time, it does not seem possible to draw any firm conclusion about the agreement or disagreement of linked-cluster and variational methods.

ACKNOWLEDGMENTS

This work has greatly benefitted from discussions and correspondence with B. Brandow, F. Coester, M. T. Johnson, A. Kallio, E. Krotscheck, H. Kümmel, J. W. Negele, V. R. Pandharipande, S. C. Pieper, R. A. Smith, R. B. Wiringa, and especially J. W. Clark and B. D. Day, through innumerable comments and suggestions which we hereby gratefully acknowledge.

*Supported by U. S. ERDA, Division of Physical Research and the Deutsche Forschungsgemeinschaft.

†Present address: Institut für Theoretische Physik II, Ruhr-Universität, D-4630 Bochum, Fed. Rep. Germany.

[1]J. W. Clark (unpublished).
[2]S.-O. Bäckman, J. W. Clark, W. J. Ter Louw, D. A. Chakkalakal, and M. L. Ristig, Phys. Lett. 41B, 247 (1972); S.-O. Bäckman, D. A. Chakkalakal, and J. W. Clark, Nucl. Phys. A 130, 635 (1969).
[3]B. H. Brandow, Phys. Rev. 152, 863 (1966); H. A. Bethe, Ann. Rev. Nucl. Sci. 21, 93 (1971).
[4]S. Fantoni and S. Rosati, Nuovo Cimento Lett. 10, 545 (1974); Nuovo Cimento 25A, 593 (1975).
[5]E. Krotscheck and M. L. Ristig, Phys. Lett. 48A, 17 (1974); Nucl. Phys. A 242, 389 (1975).
[6]J. G. Zabolitzky, Phys. Lett. 64B, 233 (1976).
[7]V. R. Pandharipande, R. B. Wiringa, and B. D. Day, Phys. Lett. 57B, 205 (1975).
[8]R. Jastrow, Phys. Rev. 98, 1479 (1955).
[9]D. Ceperley, G. V. Chester, and M. H. Kalos, Phys. Rev. B (to be published).
[10]R. V. Reid, Ann. Phys. (N.Y.) 50, 411 (1968).
[11]V. R. Pandharipande and R. B. Wiringa, Nucl. Phys. A 266, 269 (1976).
[12]M. Gaudin, J. Gillespie, and G. Ripka, Nucl. Phys. A 176, 237 (1971).
[13]J. M. J. van Leeuwen, J. Groeneveld, and J. de Boer, Physica 25, 792 (1959); T. Morita, Prog. Theor. Phys. 20, 920 (1958).
[14]E. Feenberg, *Theory of Quantum Fluids* (Academic, New York, 1969).
[15]V. R. Pandharipande and H. A. Bethe, Phys. Rev. C 7, 1312 (1973).
[16]R. A. Smith, Phys. Lett. 63B, 369 (1976).
[17]V. R. Pandharipande and K. E. Schmidt (unpublished).
[18]F. Iwamoto and M. Yamada, Prog. Theor. Phys. 18, 345 (1957).
[19]H. W. Jackson and E. Feenberg, Ann. Phys. (N.Y.) 15, 266 (1961).
[20]J. W. Clark and P. Westhaus, Phys. Rev. 141, 833 (1966); 149, 990 (1966).
[21]E. Krotscheck and K. Takahashi, Phys. Lett. 61B, 393 (1976).
[22]J. W. Clark, M. Johnson, P. M. Lam, and J. G. Zabolitzky, Nucl. Phys. (to be published).
[23]H. Kümmel, Z. Phys. 279, 271 (1976).
[24]V. R. Pandharipande, Nucl. Phys. A 178, 123 (1971); 181, 33 (1972).
[25]J. W. Clark and M. L. Ristig, Phys. Rev. C 7, 1792 (1973); D. A. Chakkalakal, C.-H. Yang, and J. W. Clark, Nucl. Phys. A 271, 185 (1976).
[26]H. B. Keller, *Numerical Methods for Two-Point Boundary Value Problems* (Blaisedell, London, 1968).
[27]J. M. Ortega and W. C. Rheinboldt, *Iterative Solution of Nonlinear Equations in Several Variables* (Academic, New York, 1970).
[28]D. Schiff and L. Verlet, Phys. Rev. 160, 208 (1967).
[29]F. Y. Wu and E. Feenberg, Phys. Rev. 128, 943 (1962).
[30]K. R. Atkin, *Liquid Helium* (Cambridge U.P., Cambridge, England, 1959).
[31]S. Fantoni and S. Rosati, Nuovo Cimento Lett. 16, 531 (1976).
[32]L. Shen, H.-K. Sim, C.-W. Woo, Phys. Rev. D 10, 3925 (1974).
[33]O. Benhar, C. Ciofi degli Atti, S. Fantoni, S. Rosati, A. Kallio, L. Lantto, and P. Toropainen, Phys. Lett. 64B, 395 (1976).
[34]B. D. Day (private communication).
[35]E. K. Achter and L. Meyer, Phys. Rev. 188, 291 (1969).
[36]B. H. Brandow, Phys. Lett. 61B, 117 (1976).
[37]E. Krotscheck (unpublished).
[38]E. Krotscheck, J. Low Temp. Phys. 27, 199 (1977).
[39]H. Kümmel, K. H. Lührmann, and J. G. Zabolitzky, Phys. Rep. (to be published).
[40]B. D. Day (private communication).
[41]R. B. Wiringa and V. R. Pandharipande (private communication).
[42]C. C. Chang and C. E. Campbell, Phys. Rev. B 15, (1977); F. J. Lee and D. K. Lee (unpublished).